Input-specific bi-directional regulation of CA3 pyramidal cell excitability: implication in sequential memory formation

Kisang Eom[1,3] Yujin Kim[1,2], Seungmin Baek[1], Alan J Park[1], Won-Kyung Ho[1], Suk-Ho Lee[1,2,4*]

[1] Department of Physiology, Seoul National University College of Medicine, 103 Daehak-ro, Jongno-gu, 03080, Seoul, Republic of Korea.

[2] Department of Brain and Cognitive Science, Seoul National University College of Natural Science, 103 Daehak-ro, Jongno-gu, 03080, Seoul, Republic of Korea.

[3] Current address: Department of Physiology, Keimyung University School of Medicine, 1095 Dalgubeol-daero street, Dalseo-gu district, Daegu, Republic of Korea.

[4]Lead Contact

*****Correspondence**:** Suk-Ho Lee: leesukho@snu.ac.kr

Funding information

National Research Foundation of Korea, Grant/Award Number: 2020R1A2C2006438

Summary

Neuronal excitability is a key determinant for recruitment of a neuron to an ensemble. High-frequency mossy fiber (MF) inputs induce prolonged increases in the excitability of a CA3 pyramidal cell (long-term potentiation of intrinsic excitability, LTP-IE), which primes the cell such that weak perforant pathway (PP) inputs can induce long-term potentiation at PP synapses (PP-LTP). However, sustained hyperexcitability can be detrimental, and a mechanism to reverse this state is necessary. Here, we show that burst firings of CA3 pyramidal cells elicited by PP or recurrent inputs reverse the MF-induced LTP-IE. Moreover, the high-frequency PP inputs to CA3-PCs already primed by MF inputs induced not only PP-LTP but also restored the high excitability state. Labeling neuronal ensemble using c-fos promoter in animals exposed to a novel context, we found most CA3 ensemble cells exhibited increased excitability, indicative of LTP-IE. Moreover, when the animals experienced novel contexts twice with a 30 min interval, a substantial subset of putative twice-activated CA3 ensemble cells exhibited reduced excitability, implying depotentiation of LTP-IE. We developed an in silico model based on the experimental results and found that MF-induced LTP-IE and its depotentiation are critical for the association of neuronal ensembles representing temporally spaced events.

Introduction

Hippocampal CA3 pyramidal cells receive two kinds of extrinsic synaptic inputs from dentate gyrus (DG) and entorhinal cortex (EC) via mossy fibers (MFs) and perforant pathway (PP), respectively. MF, an axon of granule cell in DG, makes sparse, strong and non-Hebbian synaptic connections to proximal dendrites of hippocampal CA3-PCs (Henze et al., 2002), whereas PP makes a much larger number of weak Hebbian synapses on distal dendrites of CA3-PCs. Computational models based on these features predicted that MF inputs contribute to orthogonal encoding, while PP inputs are required for cued memory retrieval of a pattern stored in the CA3 recurrent network (Treves and Rolls 1992; O'Reilly and McClelland, 1994). This prediction was supported by behavioral studies (Hunsaker & Kesner, 2013; Lee & Kesner, 2004). Involvement of PP synapses in retrieval of episodic memory implies that long-term plasticity (LTP) at PP synapses would play a key role in triggering reactivation of CA3 ensembles from auto-associative CA3 network during retrieval. Because PP synaptic inputs are not strong enough to drive firing of CA3-PCs, MF-driven firing would be required for induction of Hebbian LTP at PP synapses (McNaughton and Morris, 1987). Previously, however, we found that high frequency MF inputs not only provide such immediate depolarization but also induce sustained enhancement of dendritic voltage responses to PP synaptic inputs, called long-term potentiation of intrinsic excitability (LTP-IE) (Eom et al., 2019; Hyun et al., 2015; Hyun et al., 2013). The MF-induced LTP-IE is mediated by an increase in the distal apical dendritic excitability (Hyun et al., 2013), and enhances the EPSP-to-spike (E-S) coupling of PP inputs (Hyun et al., 2015). The potentiation of E-S coupling (E-S potentiation) facilitates homosynaptic LTP at PP synapses (Eom et al. 2022). Because LTP-IE is not a synapse-specific process but occurs over a whole distal dendritic arbor, LTP-IE without depotentiation would lead to rapid saturation of PP-CA3 synaptic weights, which will causes impairment of further learning (Moser et al., 1998), and excitation/inhibition imbalance of recurrent network activity. It remains unexplored, however, how MF-induced high excitability state of CA3-PC is restored to the baseline.

The other question to be addressed is whether LTP-IE indeed occur CA3-PCs that participate in neuronal ensembles (called CA3 ensemble cells) *in vivo*. This question is crucial to understand CA3 ensemble dynamics because neuronal excitability is a key factor that determines whether a given neuron is recruited to an ensemble carrying information. Once a CA3-PC receives high-frequency MF inputs and undergoes LTP-IE (referred to as MF-induced priming) in a previous episode, the probability for the primed cell to be recruited to an ensemble in the next episode would be enhanced because PP input alone can drive firing

in the primed CA3-PC. Whereas dynamic changes of intrinsic excitability accompanied with behavioral learning have been explored in hippocampal DG and CA1 area (Oh & Disterhoft, 2015; Pignatelli et al., 2019),the same issue in the CA3 region remains unexplored.

The present study was set out to address these two questions. Here, we show that MF input-induced primed state of a CA3-PC is terminated by high-frequency PP or associational/commissural (A/C) inputs. Moreover, CA3 ensemble cells exhibited indeed high excitability features similar to CA3-PCs that underwent LTP-IE, and LTP-IE was reversed in a subset of putative twice-activated CA3 ensemble cells when an animal experienced two temporally separated events.

Hippocampal CA3 has been implicated not only in non-overlapping representation of episodic memories but also in the memory of sequence of temporally discontiguous events (Farovik et al., 2010). Recently, the synaptic tagging and capture hypothesis and/or post-learning cAMP response element binding protein (CREB)-dependent modification of intrinsic excitability have been proposed as network mechanisms that permit the overlap of ensembles representing temporally separate episodes in hippocampal CA1 and amygdala (Lisman et al., 2018). This overlap may be mediated by increased sharing of feedforward inputs between the ensembles because recurrent connections between principal cells lack in these areas. The same regulation of ensemble overlap in a recurrent network would have a detrimental effect on the orthogonality of ensembles because co-active neurons tend to be strongly connected via recurrent synapses (called auto-association), which may eventually lead to a merge of ensembles. Therefore, different mechanisms may be necessary in order for two orthogonal ensembles to be associated (called hetero-association) in a recurrent network, but it is little understood. Incorporating in vitro findings to the Hebb-Marr CA3 network model (McNaughton & Morris, 1987), we propose that the MF- and PP-induced bi-directional regulation of CA3-PC excitability may link two orthogonal ensembles representing two events adjacent in a sequence even if they are temporally separated, while it does not allow further hetero-association between ensembles carrying information non-adjacent events in a sequence. Therefore, the learning rule proposed in the present study may subserve formation of sequential memory in the CA3 network.

Materials and Methods

Animals and ethical approval. All studies, experimental protocols, and animal manipulation protocol described in this article were conducted with the Institutional Animal Care and Use Committee (IACUC). The animals were maintained in standard environmental conditions (Temperature: 25 ± 2 ºC, Humidity: 60 ± 5 %, Dark/Light cycle: 12/12h) and monitored under veterinary supervision by Institute for Experimental Animals, Seoul National University College of Medicine.

Stereotaxic surgery and intrahippocampal injection of adeno-associated virus (AAV) for ex vivo study. An adeno-associated virus (AAV-RAM-d2TTATRE-EGFP-WPRE-pA, titer: 4.8×10^{12} GC/ml) was manufactured by KIST virus facility (Seoul, Republic of Korea). Surgery was performed on young-adult SD rats (6 weeks). Before stereotaxic injection of the AAV into hippocampus, animals were singly housed to new homecage for 1 week to acclimation with doxycycline diet (40 mg/kg). Animals were kept on the doxycycline diet and allowed to recover for at least 7 days following surgery. After anesthesia with isoflurane, rats were secured in a stereotaxic frame (Neurostar, Tubingen, Germany). Holes were drilled bilaterally in the skull at the injection sites (2 sites). Stereotaxic coordinates used for intrahippocampal injections were as follows (from bregma); for a ventral hippocampus, anterior–posterior -2.85 mm, mediolateral ±2.8 mm, dorsoventral 3.3 mm. A 33-gauge needle attached to a 50 µl Hamilton syringe (#80908), mounted to the stereotaxic frame, and under control of a microinjection syringe pump UMP3T-1 controller (WPI, Sarasota, FL, USA) was used to inject 0.8 µl of AAV at each site. Injections occurred at a rate of 0.08 µl/min, after which the needle was left in place for an additional 2 min. After injections were completed, the skin was sutured and the animals were allowed to recover for 1 h on a heating pad before returning to the home cage. Mice remained in the homecage for an additional 2 weeks to recover before the start of behavioral testing and post-hoc *ex vivo* experiments. The diet was switched to doxycycline-free diet 2 days before contextual fear conditioning (CFC) to allow tetracycline transcriptional activator (tTA) to activate the tTA-responsive element (TRE) promoter driving expression of EGFP.

B6.Cg-Tg(Fos-tTA,Fos-EGFP*)1Mmay/J mice. cfos-tTA/cfos-shEGFP mice were purchased from Jackson laboratory (stock No: 018306; Donating investigator: Mark Mayford, The Scripps Research Institute, La Jolla, CA), and crossed to the C57BL/6J background to maintain lineage. The cfos-shEGFP transgenes allows us to quantify c-fos expression correlated with neuronal activation by measuring fluorescence of short half-life green fluorescent protein (shEGFP, $t_{1/2}$ = 2 hours). For genotyping, DNA was isolated from the tail of each mouse in the litter aged 6 ~ 8 days as the method provided by the Jackson Laboratory

122 (https://www.jax.org/strain/018306). All animals were maintained in the standard environmental
123 conditions described above.

124 **Exposure of animals to a novel context.** The cfos-tTA/cfos-shEGFP mice (hereafter cfos-EGFP mice) of
125 either sex (6-8 weeks old) were singly housed for 1 weeks before the experiments. On the experimental
126 day, the mice were placed in novel contexts; context A or A and B. Context A is a chamber (18 cm wide ×
127 18 cm long × 30 cm high; H10-11M-TC; Coulbourn Instruments 5583, PA 18052, USA) consisting of a metal
128 grid floor, aluminum side walls, and a clear Plexiglass front door and back wall. The context A chamber
129 was lit indirectly with a 12 W light bulb. The features of context B were the same as context A, except for
130 a unique odor (1% acetic acid), dimmer light (50% of A), and a slanted floor by 15° angle. The chamber
131 and cage were cleaned using 70% ethanol before placing an animal and between each runs. In context A,
132 but not in context B, animals were allowed a 3-min exploration, received a single foot shock (0.7 mA, for
133 2 s) and were returned to their home cage 60 s after the shock. In the context B, animals were allowed a
134 5-min exploration and returned to their homecage.

135 **Preparation of hippocampal slices.** Acute transverse hippocampal slices were obtained from Sprague-
136 Dawley rats (PW2-3 for Figures 1-4 and Figures S2-S3; PW6 for Figure 5; PW, postnatal weeks) or cfos-
137 shEGFP mice (PW6-8 for Figures 6-7) or ZnT-heteroKO and ZnT-heteroKO/cfos-shEGFP mice (PW6, Figure
138 8) of either sex. Animals were anesthetized by inhalation of isoflurane. After decapitation, brain was
139 quickly removed and chilled in ice-cold preparation solution containing 75 sucrose, 87 NaCl, 25 $NaHCO_3$,
140 2.5 KCl, 1.25 NaH_2PO_4, 25 D-glucose, 7 $MgCl_2$, and 0.5 $CaCl_2$ (in mM; equilibrated with carbogen mixture
141 of 95% O_2 and 5% CO_2). After mounting on a slicer (Leica VT1200, Nussloch, Germany), 300 µm (whole-
142 cell recording)-thick transverse slices (whole-cell recording) were prepared and incubated at 34 ºC for 30
143 min in the preparation solution, and thereafter stored at room temperature (22 ºC). For experiments,
144 slices were transferred to a submersion recording chamber superfused with standard aCSF containing 124
145 NaCl, 26 $NaHCO_3$, 3.2 KCl, 1.25 NaH_2PO_4, 10 D-glucose, 2.5 $CaCl_2$, and 1.3 $MgCl_2$ (in mM).

146 **Confocal microscopy and image quantification.** We tested 4 cfos-shEGFP mice (PW6-8) between 8 and
147 14 weeks of age for contextual exposure. Before the experiments, mice were a singly housed to new
148 homecage for 1 week for acclimation. For experiments depicted in Fig. S4, mice were divided into two
149 groups: exposure of context A only and waiting in homecage for 90 min (ctxA), exposure of context A and
150 B with 25-min interval and waiting in homecage for 60 min (ctxAB). Two groups were sacrificed to prepare
151 hippocampal slices after 90 min from the exposure of ctxA, as aforementioned. Confocal images from the

152 hippocampal slices in Fig. S4 were obtained in the submerged recording chamber that was continuously
153 perfused with the recording solution at 1.5 ml/min. To suppress unnecessary neural activity, picrotoxin
154 (10 µM) and CNQX (10 µM) were added to the solution. For analysis of fluorescence intensity of shEGFP(+)
155 CA3-PCs, Z-series (60-90 frames, 0.71 µm /frame) image were acquired from the live slices using a 40x
156 lens using FV 1200 confocal laser scanning microscope (Olympus, Tokyo, Japan). LD473 (15mW) laser
157 system controlled by combiner (FV10-MCPSU) was used to excite shEGFP in CA3-PCs. Typically, four
158 images were analyzed for each animal in the CA3 region. Fluorescence intensity profile for each shEGFP(+)
159 CA3-PCs based on depth from surface of slices were obtained from Z-stack image of CA3 region. The
160 surface of hippocampal slices was defined as 0 µm of depth in hippocampal slices. We regarded
161 fluorescence signals that is above a threshold of 5× the SD of baseline fluctuation of signal intensity profile
162 as the signal of shEGFP(+) CA3-PCs. The depth for the maximal fluorescence intensity was defined as the
163 depth of CA3-PCs.

164 **Epifluorescence imaging for AAV-injected rats or cfos-shEGFP mice.** Fig. 5 and 6 ~ 8 depict ex vivo
165 electrophysiological studies of CA3-PCs obtained from AAV-injected rats and cfos-shEGFP mice,
166 respectively. After acclimation of 1 weeks, AAV-injected rats were exposed to context A once for 5 min
167 and returned to homecage for 1, 1.5, and 3 hours (Fig. 5) and sacrificed to obtain brain slices. cfos-shEGFP
168 mice were divided into several groups: exposure of context A only and waiting in homecage for 60 min
169 (ctxA60), exposure of context A only and waiting in homecage for 90 min (ctxA90), and exposure of
170 context A and B with 25-min interval and waiting in homecage for 60 min (ctxAB). ctxA60 and ctxA90
171 groups were sacrificed to prepare brain slices after 60 min and 90 min from the exposure of context A.
172 For ctxAB group, animals were sacrificed to obtain brain slices after 60 min from the exploration of last
173 context, context B. EGFP or shEGFP was excited at 488 nm light with a monochromator (Polychrome IV,
174 xenon-lamp based, Polychrome-V, TILL-Photonics, Martinsried, Germany) and visualized using a 520/535-
175 nm band-pass emission filter (Fig. 5 and 6). In experiments for Fig. 6 - 8, to adjust deviation of fluorescence
176 intensity of shEGFP caused by the optical path length, 50 µM Alexa flour 594 (AF594) was added to
177 intracellular solution and loaded to CA3-PCs during whole-cell configuration. AF594 was excited at 594
178 nm light with the monochromator and visualized using a 660 nm long-pass emission filter. Acquired
179 images were analyzed with HC-Image Live 4.0 (Hamamatsu Photonics, Shizuoka, Japan). Whole-cell
180 recordings (WCR) were performed under the IR-DIC (Fig. 5Ab). WCR of EGFP(-) cells were used as control
181 and compared to recording of EGFP(+) or shEGFP(+) cells. The fluorescence intensity in the wide-field
182 epifluorescence image was set with manually-adjusted ROI based on the contour of cells.

183 **Electrophysiological study.** Whole-cell voltage- or current-clamp recordings from CA3-PCs were
184 performed at near-physiological temperature (34 ± 1 ºC), while the recording chamber was perfused with
185 the standard aCSF at 1 ~ 1.5 ml/min. Patch pipettes were pulled from borosilicate glass tubing (outer
186 diameter: 1.5 mm, wall thickness: 0.225 mm) with a horizontal pipette puller (P-97, Sutter Instruments,
187 Novato, CA, USA) and filled with the intracellular solution containing 130 K-gluconate, 7 KCl, 1 $MgCl_2$, 2
188 Mg-ATP, 0.3 Na-GTP, 10 HEPES, 0.1 EGTA (in mM; pH adjusted to 7.20 with KOH, 295 mOsm) with the
189 pipette resistance was 3 ~ 4 MΩ. After formation of whole-cell configuration on the somata of CA3-PCs,
190 recordings were performed from only those cells that had stable resting membrane potential within -76
191 and -58 mV (cells that had more positive resting membrane potential or unstable resting membrane
192 potential were discarded). Under this condition, input conductance (G_{in}) was measured from subthreshold
193 voltage responses to -30 pA and +10 pA current steps of 0.5 s (Hyun et al., 2015). G_{in} was monitored every
194 10 s before and after delivery of a conditioning protocol. Recordings were obtained in the presence of a
195 $GABA_A$ receptor antagonist, picrotoxin (PTX, 100 µM) unless specified. All recordings were made using a
196 MultiClamp 700B amplifier controlled by Clampex 10.2 through Digidata 1440A data acquisition system
197 (Molecular Devices, Sunnydale, CA, USA). Also, we stimulated different types of synapses on CA3-PCs to
198 evaluate the influence of each synaptic input on the intrinsic excitability of CA3-PCs. Afferent PP fibers
199 were stimulated with a concentric bipolar electrode (CBAPB125; FHC Inc., Bowdoin, ME, USA) positioned
200 at SLM on the border of the subiculum and CA1 (for PP stimulation)(Perez-Rosello et al., 2011).
201 Associational/commissural (A/C) fibers were stimulated with a glass micro-pipette placed on alveus. Brief
202 stimulation pulses (0.1 ms) were generated by a computer-controlled digital stimulator (DS8000, WPI;
203 Sarasota, FL, USA) and delivered to a stimulation electrode through an isolation unit (DLS100 stimulus
204 isolator, WPI). For extracellular recording, field excitatory postsynaptic potentials (fEPSPs) were recorded
205 from striatum lacunosum-moleculare (SLM) of CA3 by a glass electrode filled with 150 mM NaCl
206 (resistance, c.a. 1 MΩ).

207 *Simulation methods*

208 **Simulation methods.** We considered a recurrent network comprised of 1000 PCs and 200 INs, in which
209 PCs and INs are numbered with indices from 1 to 1000, and those from 1001 to 1200, respectively. Initial
210 connectivity matrix (*W*) are shown in Fig. S5A. The connectivity, defined as the probability that an element
211 of *W* has nonzero value, was set to 10% for synaptic connections between PCs, while the connectivity
212 between CA3 PCs is less than 2% *in vivo* (Guzman et al., 2016). This high connectivity partially compensates
213 lower recurrent synaptic inputs from a given ensemble compared to the real rat CA3 network. The firing

property of neurons was simulated by the leaky integrate and fire model as described in detail elsewhere (Yoon et al., 2020). The resting membrane potential (V_L) and the firing threshold (V_θ) were set to -65 and −55 mV, respectively, for both CA3-PCs and GABAergic interneurons (INs). To model recurrent and inhibitory synaptic inputs, we assumed that firing of a presynaptic CA3 PC or IN (denoted by subscripts 'e' and 'i', respectively) induces an instantaneous increase in the postsynaptic conductance by G_s after a synaptic delay, D_s, where $s \in \{e, i\}$ (D_e = 2 ms; D_i = 1 ms), and that the decay of the conductance change follows a mono-exponential function with a time constant τ_s ($\tau_e = \tau_i$ = 10 ms) (Guzman et al., 2016; Kohus et al., 2016). Multiple synaptic inputs to a neuron, *j*, were linearly summated. When the number of *s* type presynaptic neurons innervating postsynaptic neuron, *j*, is K_s, the dynamics of subthreshold membrane potential of the neuron, *j*, is assumed to follow the equations:

$$\tau_m \, dv_j(t)/dt = -(v_j - v_L) - (1/G_m) \, \Sigma_{s=\{e,i\}} \Sigma_{k=(1..Ks)} \, [G_{s,jk} (v_j - E_s) \, S_{s,jk}]$$

$$\tau_s \, dS_{s,jk}/dt = - S_{s,jk} + \Sigma_{t_{AP}} \, \delta(t - t_{AP} - D_s)$$

, where τ_m = cell membrane time constant; G_m = passive membrane conductance (5 nS for PCs and INs); $G_{s,jk}$ = synaptic conductance of synaptic type, *s*, from a neuron *k* to *j*; E_s = reversal potential of synapse type (E_e = 0 mV, E_i = -68 mV). The $S_{s,jk}$ is an activation parameter for synaptic type *s* from a neuron *k* to *j*. It is activated by presynaptic firing at t_{AP}, and undergoes mono-exponential decays with a time constant, τ_s. When membrane potential (*v*) surpasses the threshold potential (V_θ), the *v* was reset to -55 mV. To simulate a post-spike refractory period, the V_θ was increased to -15 mV just after firing, which undergoes mono-exponential decay with time constants of 50 and 15 ms for PC and INs, respectively. The summation of external excitatory synaptic inputs via MF and PP were calculated in the same manner as recurrent excitatory inputs, but the arrival of external synaptic inputs was pre-determined as a patterned input as shown in Fig. 9Ba. We assumed that four input patterns arrive at t = 0, 0.8 s, 1.8 s and 3 s in a series. The synaptic conductance values for MF and PP inputs to PCs were set to 20 and 0.3 nS, and those to INs were 4 and 0.15 nS, respectively. The decay time constants of MF and PP inputs were set to 4 and 17 ms (Hyun et al., 2015; Jonas et al., 1993). At the start of simulation, membrane potential of all neurons was initialized to -65 mV. The voltage derivative (dv/dt) of each neuron was calculated with a time step of 0.4 ms, and was numerically integrated by Euler methods using Matlab software (R2021a, Mathworks, USA). During encoding phase, the recurrent and PP synaptic weights were modified under the STDP rules. The dependence of LTP level on the spike timing difference between pre and post-synaptic cells ($\Delta t = t_{post} - t_{pre}$) is shown in Fig. S5Ba-Bb.

Assumptions for the CA3 network model

Assumptions for the CA3 network model. We consider an animal, which experience a series of episodes. We call MF and PP afferent inputs to CA3-PCs carrying the information of *i*-th episode as *i*-th pattern ($\boldsymbol{P}_i$).

1. *MF inputs are strong and sparse, while PP inputs are weak and diffuse*: Only a small and non-overlapping subset of CA3-PCs receive MF input during encoding (or learning) phase, while almost all CA3-PCs receive PP inputs with different strength. Henceforth, a group of CA3-PCs that receive MF inputs carrying information of the *i*-th pattern ($\boldsymbol{P}_i$) will be denoted as $\mathbf{M}_i$ subset.
2. *Distributions of MF and PP input strength are skewed*: During encoding phase, the MF input strength to CA3-PCs of a given **M** subset follows a log-normal distribution (Buzsaki & Mizuseki, 2014). We assumed that a small fraction of CA3-PCs in a given **M** subset receive strong MF inputs, in which LTP-IE is induced by concerted actions of intracellular Ca^{2+} and Zn^{2+} signaling (Eom et al., 2019). A subset of CA3-PCs that underwent LTP-IE during encoding of $\boldsymbol{P}_i$ will be denoted as $\mathbf{M}_i$*.
3. *LTP at A/C and PP synapses requires converging MF inputs*: Because A/C and PP synapses display Hebbian plasticity (McMahon & Barrionuevo, 2002; Mishra et al., 2016; Tsukamoto et al., 2003)), LTP at A/C and PP synapses is critically dependent on the postsynaptic firing. Sparse and strong MF input provides an additional variance in the excitatory input distribution over the CA3-PC population and thus governs the firing pattern of CA3-PCs during a learning phase under competitive *k*-Winners-Take-All regime (O'Reilly & McClelland, 1994; Treves & Rolls, 1992). Moreover, acetylcholine (Ach) level is high during encoding phase, and the high Ach reduces the A/C synaptic strength by 50% (Hasselmo, 2006; Vogt & Regehr, 2001). As a result, LTP at A/C and PP synapses is supervised by MF inputs that carry information of an episode. The memory for *i*-th episode ($\boldsymbol{E}_i$) is stored at PP and A/C synapses of CA3-PCs comprising $\mathbf{M}_i$ subset (referred to as $\mathbf{M}_i$ PCs).

Data Analysis

Data analysis. Electrophysiological data were acquired and digitized using an analogue-to-digital converter (Digidata 1440A, Molecular Devices) and stored in a computer hard disk. Analyses of data were performed with Igor Pro (version 6.10A; WaveMetrics, Lake Oswego, OR, USA) and Clampfit 10.2 (Molecular Devices, Sunnyvale, CA, USA). We used the bias-corrected version of Akaike information criterion (AIC) to select a better distribution model for the histogram data of fluorescence intensities in Fig. S4D (Hurvich & Tsai, 1989). Statistical data are expressed as mean ± standard error of the mean (SEM), and the number of cells measured (denoted as *n*). Statistical data were evaluated for normality and

274 variance equality with Kolmogorov-Smirnov test and Levene's test, respectively. For data that satisfy
275 normality and equality of variances, statistical evaluations were performed with Student's t-test or
276 general linear model (GLM). For data that did not satisfied above properties, nonparametric tests, such as
277 Mann-Whitney U test or Wilcoxon signed rank test, were performed to evaluation. For simplicity of
278 description, significance level (P) was marked as $P < 0.05$. n.s., no statistical significance; $^{*}P < 0.05$; $^{**}P <$
279 0.01; $^{***}P < 0.005$ in figures. Statistics processing was performed with PASW Statistics 18 (SPSS Inc, 2009,
280 Chicago, IL, USA).

281

282

Results

Differential effects of intracellular glutathione (GSH) on somatic and MF-induced LTP-IE

The LTP-IE is mediated by Ca^{2+} and protein tyrosine kinase (PTK)-dependent downregulation of Kv1.2, which is antagonized by receptor protein tyrosine phosphatase alpha (RPTPα). RPTPα is activated by PKC, and inactivated by oxidative stress and Zn^{2+} (Fig. S1) (Eom et al., 2019) (Blanchetot et al., 2002; Meng et al., 2002). Reducing molecules such as NADH and reduced form of glutathione (GSH) are normally present in cytosol in millimolar range (Forman et al., 2009). Intracellular perfusion with the conventional whole-cell patch pipette solution lacking reducing molecules may bias the cellular redox state to oxidized state. To prevent inactivation of protein tyrosine phosphatase (PTP) during whole-cell recording (WCR), we added 5 mM GSH to the pipette solution. We confirmed that input conductance (G_{in}) and PP-evoked EPSPs (PP-EPSPs) were stable up to 45 min of WCR in the presence of 5 mM GSH (Fig. S2). The latency of the first action potential (1st AP latency, Fig. S2Ca-Cb) and AP threshold (Fig. S2Cc) measured by a ramp current injection (250 pA/s) were not different between at 5 min and at 45 min of WCR. Henceforth, all the whole-cell patch experiments shown in Fig. 1-4 were done using pipette solution containing GSH, unless stated otherwise.

The long lasting increases in input resistance (inverse of G_{in}) and PP-EPSPs are the hallmarks of LTP-IE in CA3-PCs, which can be induced by 10 Hz somatic AP firing (somatic conditioning) or 20 Hz MF stimulation (MF conditioning)(Eom et al., 2019; Hyun et al., 2015; Hyun et al., 2013). After measuring the baseline G_{in} for 5 min, the somatic or MF conditioning was delivered (black or red arrowhead, respectively). The G_{in} of CA3-PCs decreased until 10 min after either of somatic and MF conditioning (Fig. 1Aa-Ac). Without GSH, G_{in} was kept reduced longer than 30 min after somatic conditioning (Hyun et al., 2013). In the presence of intracellular GSH, however, G_{in} returned to the baseline in 30 min after somatic conditioning. In contrast, the G_{in} after MF conditioning stayed low throughout 30 min recordings (Fig. 1Aa-Ac). The 1st AP latency measured from ramp current responses was accelerated in parallel with the change of G_{in} (Fig. 1Ad-Ag). The G_{in} reduction was always accompanied by an increase in PP-EPSPs. PP-EPSPs rapidly increased in 3 min after the conditioning as previously observed (Hyun et al., 2015) (Fig. 1Ba-Bc). However, the PP-EPSP amplitudes after somatic conditioning rapidly returned to the baseline over 5-10 min, but those after the MF conditioning stayed enhanced during the 30 min recording (Fig. 1Ba-Bc). Neither somatic nor MF conditioning altered the amplitude of PP-EPSCs (Fig. 1Bd-Be). EPSC amplitude depends on neurotransmitter release and AMPA receptor expression but not on intrinsic excitability. Thus, these

313 results suggest that MF inputs augment CA3 dendritic excitability thereby increasing PP-EPSPs. Given that
314 PTP activity is preserved by GSH in the pipette solution, our results suggest that PTP may rapidly reverse
315 the LTP-IE induced by somatic conditioning but not that by MF conditioning.
316 Why MF-induced LTP-IE is not spontaneously reversed unlike LTP-IE induced by somatic conditioning? This
317 question can be addressed in light of our previous findings that MF conditioning induces not only Ca^{2+} but
318 also Zn^{2+} signaling, and the latter facilitates LTP-IE by reversible inhibition of PTP (Eom et al., 2019).
319 Somatic conditioning which induces Ca^{2+} transients (CaTs) without Zn^{2+} signaling, however, may activate
320 both PTKs and PTPs (Brandt et al., 2003; Eom et al., 2019; Lev et al., 1995; Tsai et al., 1998), and lead to
321 the short-lasting potentiation of intrinsic excitability (PIE). This result is in stark contrast to our previous
322 observation that somatic conditioning readily induced long-lasting PIE in the absence of GSH (Hyun et al.,
323 2013), and suggests a possibility that MF-induced LTP-IE may be reversed by activation of PTP by a Ca^{2+}
324 transient without Zn^{2+} signaling.

325

326 *Depotentiation of MF-induced potentiation of PP-fEPSPs by A/C synaptic stimulation*

327 We hypothesized that CaTs without Zn^{2+} signaling may reverse MF-induced LTP-IE when the activity of
328 PTP is preserved. CaTs without Zn^{2+} signalling can be evoked by stimulation of soma or afferent fibers
329 other than MFs (non-MF) such as PP or associational/commissural (A/C) fibers (Eom et al., 2019). To
330 prevent perturbation of the intracellular milieu of CA3-PCs, we monitored PP-evoked field EPSPs (PP-
331 fEPSPs) before and after MF conditioning and subsequent A/C fiber stimulations. The recording and
332 stimulating electrodes were placed as shown in Fig. 2Aa (see Materials and Methods). Stimulation of PP
333 evoked a negatively deflecting fEPSP at the recording electrode placed in stratum lacunosum-moleculare
334 (SLM) (gray-black, Fig. 2Ab), while stimulation of MFs (cyan) and A/C fibers (red) evoked positive fEPSP at
335 SLM. Fig. 2Ac and Ad shows the input-output relationship for the peak amplitude and initial slope of PP-
336 fEPSP, respectively. The amplitude of PP-fEPSPs was attenuated by bath application of DCG-IV, an agonist
337 of group II metabotropic glutamate receptor, which is highly expressed in PP (Shigemoto et al., 1997)(Fig.
338 2Ba). The latency of PP-fEPSPs (time from PP stimulation to the peak of PP-fEPSP) was not altered by the
339 increase in stimulation intensity (Fig. 2Bb). To evoke antidromic firing of CA3-PCs and activate A/C
340 synapses, we placed a glass stimulation electrode on the alveus of CA3 (Fig. 2Bc). Stimulation of alveus
341 with 40 pulses for 2 s induced AP bursts following EPSP summation in the CA3-PC under WCR (Fig. 2Bd).

342 Both EPSPs and AP bursts were abolished by bath application of CNQX, suggesting that antidromic firings
343 of CA3-PCs activated A/C inputs to the CA3-PC under WCR, resulting in AP bursts.
344 We measured the baseline amplitude and initial slope of PP-fEPSPs evoked by paired pulses with a 100
345 ms interval before and after MF conditioning. We regarded the maximal slope over an initial half of rising
346 phase of fEPSP as initial slope of PP-fEPSP. The initial slope of fEPSP represents fast EPSC, while its peak
347 amplitudes reflects delayed activation of synaptic and somatodendritic currents (Garcia et al., 2010). MF
348 conditioning enhanced the peak amplitude of PP-fEPSP, but not the initial slope of PP-fEPSPs (Fig. 2Ca and
349 2Cb), consistent with our patch clamp results that MF conditioning enhances PP-EPSPs, but not PP-EPSCs
350 (Fig. 1). At 20 min after MF conditioning, we stimulated A/C fibers (10 pulses at 50 Hz) through the
351 electrode placed in the alveus of CA3. The peak amplitude of PP-fEPSPs gradually decreased after the A/C
352 stimulation, finally reached to the baseline (Fig. 2C). The initial slope of PP-fEPSPs and paired pulse ratio
353 (PPR) of slopes were not affected by MF and A/C conditioning (Fig. 2D), suggesting that changes in the
354 dendritic excitability of postsynaptic neurons underlie the MF-induced potentiation and nonMF-induced
355 depotentiation of PP-fEPSPs.

356

357 *MF-induced LTP-IE is de-potentiated by somatic or A/C synaptic stimulation, and is hindered by*
358 *Zn^{2+}*

359 To test whether the results of field recordings can be replicated in whole-cell recordings, we examined
360 the effects of alveus stimulation on MF-induced LTP-IE. The MF conditioning decreased the G_{in} of CA3-PCs
361 (73.5 ± 1.8%, Fig. 3Aa-Ad). The G_{in} of CA3-PCs was restored to the baseline by a train of stimuli (10 pulses
362 at 20 Hz) delivered to the alveus at 15 min after MF conditioning (Fig. 3Aa), consistent with the results of
363 field recordings (Fig. 2). Stimulation of alveus may inadvertently recruit various neuromodulator pathways
364 projecting to the CA3. We examined whether somatic AP bursts evoked by direct current injection can
365 depotentiate MF-induced LTP-IE. To this end, we adopted somatic AP bursts comprised of 10 spikes at
366 100 Hz, a typical burst firings of CA3-PCs in vivo (Kowalski et al., 2016). Somatic AP bursts at 15 min after
367 MF conditioning also restored the G_{in} to the baseline (Fig. 3Ab). To assess the minimal somatic stimulation
368 required for depotentiation of LTP-IE, we examined the effects of somatic stimulation with fewer number
369 of spikes. Surprisingly, the bursts of 2 APs at 100 Hz restored G_{in} to the baseline level (Fig. 3Ac). The
370 changes of G_{in} induced by MF conditioning and depotentiation stimulation are summarized in Fig. 3Ad.
371 Because PP-EPSP changed in parallel with G_{in} after LTP-IE induction, we evaluated whether depotentiation

372 of PP-EPSPs can be induced by somatic AP bursts. Similar to the G_{in} changes, MF-induced potentiation of
373 PP-EPSPs (197.5 ± 19.9%, Fig. 3Ba-Bd) was reversed by AP bursts elicited by alveus stimulation (Fig. 3Ba)
374 or by direct injection of ten (Fig. 3Bb) or two (Fig. 3Bc) supra-threshold current pulses at 100 Hz. The
375 amplitudes of PP-EPSCs were not altered after MF conditioning or depotentiation stimulation (time, $F_{(2,18)}$
376 = 0.017, p = 0.897; stimuli, $F_{(2,18)}$ = 0.718, p = 0.501; stimuli × time, $F_{(2,18)}$ = 0.299, p = 0.745; GLM and
377 simple effect analysis). The changes of PP-EPSPs before and after MF conditioning and depotentiation
378 stimulation are summarized in Fig. 3Bd. The lack of Zn^{2+} signaling was essential for depotentiation,
379 because somatic AP bursts did not induce depotentiation of MF-induced LTP-IE in the presence of 100 nM
380 $ZnCl_2$, which was added to aCSF 10 min after MF conditioning (Fig. 3C), supporting the notion that CaTs
381 without Zn^{2+} signaling activates PTPs and triggers depotentiation of LTP-IE.
382

383 *MF-induced LTP-IE is reversed by homosynaptic induction of LTP at PP-CA3 synapses*

384 LTP-IE potentiates PP-EPSPs, but not PP-EPSCs, because LTP-IE enhances dendritic excitability with little
385 effect on synaptic transmission *per se*. We will refer to homosynaptic LTP of PP-EPSCs as PP-LTP, distinct
386 from hetero-synaptic LTP of PP-EPSPs that occurs in parallel with MF-induced LTP-IE. The PP-CA3 synapses
387 display Hebbian plasticity (McMahon & Barrionuevo, 2002). MF-induced LTP-IE enhances E-S coupling at
388 PP synapses. Previously we showed that LTP-IE lowers the threshold of PP input strength required for
389 induction of PP-LTP (referred to as LTP threshold) in mice hippocampal CA3 (Eom et al., 2022). We
390 confirmed this notion in the rat CA3 too, with GSH-free patch pipette solution (Fig. S3 and Supplementary
391 Results).

392 Above results suggest that MF-induced LTP-IE can be reversed by somatic burst firings elicited by direct
393 somatic stimulation or A/C synaptic inputs (Fig. 2-3), and that MF-induced LTP-IE enables weak PP inputs
394 to elicit APs and induce Hebbian PP-LTP (Fig. S3). We posed a question whether AP firing elicited by weak
395 PP inputs in a MF-conditioned CA3-PC can reverse LTP-IE in the presence of GSH. We simultaneously
396 monitored PP-EPSPs (Fig. 4Aa) and G_{in} (Fig. 4Ba), while MF conditioning and subsequently weak PP-HFS
397 were delivered to induce LTP-IE and PP-LTP, respectively. MF conditioning (Fig. 4Ab) enhanced PP-EPSPs
398 but not PP-EPSCs (Fig. 4Aa), and decreased G_{in} (Fig. 4Ba). At 5 min after MF conditioning, we delivered PP-
399 HFS, which readily evoked AP firings (Fig. 4Ac) unlike naïve CA3-PCs (Fig. S3Aa). After PP-HFS, both the PP-
400 EPSPs (*left*) and PP-EPSCs (*right*) were increased (Fig. 4Ca). However, the G_{in} that had been reduced by MF
401 conditioning was restored to the baseline level (Fig. 4B). The EPSP/EPSC ratio that had been increased by

402 MF conditioning returned to the baseline after PP-HFS as shown in Fig. 4Cb. These results suggest that
403 high-frequency MF inputs prime CA3-PCs for PP-LTP expression by lowering the LTP threshold so that
404 subsequently incoming high-frequency PP inputs readily elicit AP bursts in the primed PCs. The PP-induced
405 AP bursts may lead to both PP-LTP induction and termination of MF-induced LTP-IE.

406

407 *LTP-IE occurs in hippocampal CA3 region, and lasts less than 3 hours in vivo*

408 Is the intrinsic excitability of CA3-PCs regulated in activity-dependent manner *in vivo*? We examined
409 whether LTP-IE occurs in CA3 ensemble cells activated when rats are exposed to a novel context, and if so
410 how long the enhanced excitability state is maintained. Immediate early genes (IEG) have been widely
411 used as a tool for labelling recently activated neurons. We labeled an ensemble of CA3-PCs activated by
412 contextual fear conditioning (CFC) using AAV-RAM-d2tTA-TRE-EGFP (Sorensen et al., 2016). Rats were
413 kept on doxycycline-free diet for 2 days before being subject to CFC (see Materials and Methods). Just
414 after CFC, further GFP expression was prevented by intraperitoneal injection of doxycycline (10mg/kg of
415 body weight), Then the animals were kept in their home-cage for 1, 1.5 or 3 hours before *ex vivo*
416 experiments for measuring the baseline input conductance (G_{in}) and inducibility of LTP-IE in GFP(-) and
417 GFP(+) CA3-PCs of these animals (Fig. 5Aa). About 30 min after whole-cell recordings of GFP(+) CA3-PCs,
418 we observed the diffusion of EGFP into the patch pipette (Fig. 5Ab-d). Fig. 5B shows the baseline G_{in} as a
419 function of EGFP fluorescence intensity (F_{GFP}). Most GFP(-) cells (40 out of 45 cells) showed high baseline
420 G_{in} [denoted as GFP(-/high), black symbols], but a few of them (5 cells) showed low baseline G_{in} [GFP(-
421 /low), yellow symbols]. The average baseline G_{in} values measured in GFP(+) CA3-PCs at 1 hour (red
422 symbols) and at 1.5 hours (blue symbols) after CFC were significantly lower than those of GFP(-/high) cells.
423 However, G_{in} of GFP(+) cells measured at 3 hours after CFC (green symbols) was not different from those
424 of GFP(-/high) cells. The baseline G_{in} values of GFP(-/low) cells were not different from those of GFP(+)
425 cells measured at 1 or 1.5 hours [$F_{(4,,72)} = 38.667$, $p < 0.001$; subgroups of G_{in} for the significance level of
426 0.05 are divided into two groups, GFP(-/high) and GFP(+) at 3 hours vs. GFP(+) at 1 hour, GFP(+) at 1.5
427 hours and GFP(-/low); Tukey HSD]. Assuming that ensemble cells display lower G_{in}, the GFP(-/low) cells
428 may represents non-infected ensemble cells.

429 The baseline G_{in} values for GFP(+) cells at 1 [red; GFP(+/1hr)] or 1.5 hours [blue; GFP(+/1.5hr)] after CFC
430 and those of GFP(-/low) cells were significantly lower than those of GFP(-/high) cells. Inducibility of LTP-
431 IE was evaluated by comparing baseline Gin with Gin measured at 30 min after somatic conditioning (post-

432 SC G_{in}). Somatic conditioning by 10 Hz stimulation did not induce additional decrease in G_{in} of GFP(+) and
433 GFP(-/low) cells (Fig. 5C). In contrast, LTP-IE was readily induced in GFP(+) cells at 3 hours [GFP(+/3hr)] as
434 well as GFP(-/high) cells [For GFP(-), baseline vs. post-SC, $p < 0.001$; For 3 hr, baseline vs. post-SC, $p < 0.554$;
435 GLM and simple effect analysis]. Moreover, the post-SC G_{in} values were not different between all groups,
436 suggesting that GFP(+/1hr) or GFP(+/1.5hr) after CFC and GFP(-/low) cells may have already undergone
437 LTP-IE (baseline, $F_{(3,24)} = 14.616$, $p < 0.001$; post-SC, $F_{(3,24)} = 0.706$, $p = 0.558$, GLM and univariate analysis).
438 The similarity of GFP(+/3hr) to the GFP(-/high) cells indicates that LTP-IE of CA3-PCs does not last longer
439 than 3 hours *in vivo*, and implies that there may be a mechanism that reverses the increased intrinsic
440 excitability while the animal is kept in their homecage.

441

442 *Higher GFP expression in twice-activated ensemble CA3-PCs of cfos-shEGFP mice*

443 Given that the LTP-IE of CA3-PCs is maintained at least for 90 min after CFC, we wondered whether the
444 LTP-IE can be reversed earlier by formation of a new ensemble in the CA3 area. To ensure labeling of all
445 ensemble cells, we further studied the excitability of ensemble cells using B6.Cg-Tg(Fos-tTA,Fos-
446 EGFP*)1Mmay/J mice (Jackson Stock No, 018306; referred to as cfos-shEGFP mice), which express short
447 half-life green fluorescent protein (shEGFP, $t_{1/2}$ = 2 hours) and tTA under the control of c-*fos* promoter. In
448 addition, we hypothesized that, when a neuron activated by two sequential events with a given time
449 interval, the neuron would have higher fluorescence intensity than other neurons activated by a single
450 event. To test this hypothesis, we examined distribution of fluorescence intensities of CA3-PCs from cfos-
451 shEGFP mice which visited only context A and from those which visited two contexts A and B sequentially
452 in a 30 min interval (referred to as ctxA and ctxAB mice, respectively; Fig. S4). Mice visited each context
453 for 5 min, and otherwise were kept in homecage. At 90 min after first visit, they were sacrificed for
454 preparation of brain slices. We examined fluorescence intensity of shEGFP(+) CA3-PCs located at a depth
455 less than 60 µm from the surface of hippocampal slices. Fig. S4B shows representative fluorescence
456 intensity profiles of z-stack confocal images of shEGFP(+) CA3-PCs from mice which experienced only
457 context A (72 cells, Fig. S4Ba-b) or from ctxAB (77 cells, Fig. S4Bc-Bd) mice. The scatter plot of peak
458 fluorescence intensity of each shEGFP(+) CA3-PCs as a function of its depth in the slice revealed that the
459 CA3 area of ctxAB mice harbours CA3-PCs displaying distinctly higher fluorescence intensity compared to
460 that of ctxA mice (Fig. S4C). The distribution of fluorescence intensity of shEGFP(+) CA3-PCs in either group
461 of mice showed negative skewness (Fig. S4D), indicative of log-normal (LN) distribution. The distribution

462 of CA3-PCs of ctxAB mice, but not that of ctxA mice, was better fitted by bimodal lognormal distribution
463 (Fig. S4D; AIC for mono- vs. bi-LN fits = 24.8 vs 26.6 in ctxA; 2.24 vs -9.12 in ctxAB; Note that a model with
464 lower AIC is preferred). Whereas fluorescence intensity of ctxAB cells was significantly higher than ctxA
465 cells, the distribution of low intensity groups of ctxAB largely overlapped with that of ctxA cells (Fig. S4C-
466 D), suggesting that cells of high intensity group are unique to the CA3 ensemble cells of ctxAB mice.

467

468 *LTP-IE occurs in CA3 ensemble cells and is reversed in a subset of putative twice-activated ense*
469 *mble cells*

470 Next, we examined whether the input resistance of CA3-PCs has any correlation with their epi-
471 fluorescence intensity *ex vivo* from ctxA and ctxAB mice. For ctxA mice, excitability was examined at two
472 time points: at 60 and 90 min after being kept in their home cage (Fig. 6Aa; ctxA60 and ctx90 mice,
473 respectively). The mice which experienced two contexts were kept in their homecage for 60 min, and then
474 hippocampal slices were prepared (Fig. 6Aa; called ctxAB mice). Confocal imaging of ctxA90 and ctxAB
475 slices revealed that a subset of shEGFP(+) CA3-PCs in ctxAB mice displayed distinctly higher fluorescence
476 compared to ctxA90 mice (Fig. S4), implying that such neurons may be activated twice in ctxAB mice. To
477 correct depth-dependent fluorescence attenuation in epifluorescence microscopy, we added 50 µM Alexa
478 Flour 594 (AF594; Invitrogen) to a patch pipette solution for ratiometric measurement of shEGFP and
479 AF594 fluorescence intensities. The shEGFP(+) CA3-PCs in ctxA60 and ctx90 mice were not different in
480 green-to-red fluorescence (G/R) ratios, and will be referred to as ctxA60(+) and ctxA90(+) cells,
481 respectively. Consistent with the confocal imaging results (Fig. S4), a subset of shEGFP(+) CA3-PCs from
482 the ctxAB mice displayed higher G/R ratio than the maximal G/R ratio of ctxA60(+) or ctxA90(+) cells, and
483 will be referred to as ctxAB(++) cell (Fig. 6Bc-d). The other subset which had G/R ratio similar to ctxA60(+)
484 and ctx90(+) cells, and will be referred to as ctxAB(+) cell (Fig. 6Ba-b). The G/R ratios of all shEGFP(+) cells
485 could be categorized into two groups: a group comprised of ctxA60(+), ctxA90(+) and ctxAB(+) cells and
486 the other group of ctxAB(++) cells [$F_{(3,43)}$ = 39.741, $p < 0.001$, ANOVA and Tukey HSD, Fig. 6Be]. Because
487 ctxAB(++) cells were observed only in the mice which visited context A and B, the high G/R ratio of
488 ctxAB(++) cells may be caused by double activation of c-*fos* promoter in the contexts A and B.

489 We measured G_{in} of CA3-PCs before and after somatic conditioning (2 s AP train at 10 Hz). The G_{in} for
490 GFP(-) CA3-PCs (gray) decreased after somatic conditioning (10 Hz AP train) [n = 6, GFP(-), $p < 0.001$; Fig.
491 6Ca-b]. In contrast, the baseline G_{in} values for ctxA60(+) and ctxA90(+) cells were significantly lower than

492 those of GFP(-) cells (for both cell types, $p < 0.001$), and were not further decreased by somatic
493 conditioning [ctxA60(+), $p = 0.814$; ctxA90, $p = 0.126$, Fig. 6Ca-Cb], suggesting that ctxA60(+) and ctxA90(+)
494 cells have already undergone LTP-IE while the animal visited context A. The baseline G_{in} and LTP-IE
495 inducibility of CtxAB(+) CA3-PCs were similar to those of ctxA60(+) or ctxA90(+) cells [For baseline G_{in}, $p =$
496 0.819; For pre- vs post-SC G_{in} of ctxAB(+) cells, $p = 0.873$; Fig. 6Cd-Cf]. In contrast, the excitability of
497 ctxAB(++) CA3-PCs was heterogenous. To test the inducibility of LTP-IE for ctxAB(++) cells, the ratio of
498 post-SC G_{in} over baseline G_{in} was measured. The ctxAB(++) cells were plotted on the plane of the G_{in} ratio
499 *vs.* baseline G_{in}, and clustered these data using *k*-means algorithm, yielding two clusters shown in Fig. 6Cc.
500 The low and high baseline G_{in} groups are referred to as ctxAB(++/1) cells ($n = 11$) and ctxAB(++/2) cells (n
501 $= 9$), respectively (Baseline G_{in}, $t = 4.775$, $p < 0.001$; G_{in} ratio, $t = -8.115$, $p < 0.001$). The baseline G_{in} and
502 the G_{in} ratio caused by somatic conditioning are shown as a function of G/R ratio in Fig. 6Cd and in Fig.
503 6Ce, respectively. Both baseline G_{in} -and G_{in} ratio of shEGFP(+) cells were categorized into two groups:
504 GFP(-) and ctxAB(++/2) *vs*. ctxA60(+), ctxA90(+), ctxAB(+) and ctxAB(++/1), which will be referred to as low
505 and high excitability groups, respectively [For baseline G_{in}, $F_{(5,32)} = 12.883$, $p < 0.001$; For G_{in} ratio, $F_{(5,32)} =$
506 19.565, $p < 0.001$; ANOVA and Tukey HSD]. The mean G_{in} values before and after somatic conditioning
507 are summarized in Fig. 6Cf. The baseline G_{in} values within high excitability groups were not different one
508 another, but significantly lower than the baseline G_{in} of GFP(-) cells [baseline G_{in} (gray bars), $F_{(5,31)} = 13.053$,
509 $p < 0.001$; post-SC G_{in} (red bars), $F_{(5,31)} = 1.213$, $p = 0.364$, Univariate analysis], and rather similar to the G_{in}
510 of GFP(-) cells that underwent LTP-IE ($\chi^2 = 7.279$, df = 3, $p = 0.064$, Kruskal-Wallis test).

511 The AP onset time upon injection of a short current pulse (400 - 600 pA, 8 - 12 ms; Fig. 6Da and 6Db) and
512 the latency of first AP evoked by triangular ramp current (250pA/s for 1 s; Fig. 6Dc and 6Dd) were
513 measured before and after somatic conditioning. Compared to GFP(-) cells, cells of high excitability group
514 exhibited not only lower G_{in} but also faster baseline AP onset time and the first AP latency (Fig. 6D),
515 consistent with downregulation of D-type K current (Hyun et al, 2013). The baseline AP onset time and 1st
516 AP latency of these cells were not different from those in GFP(-) cells that underwent LTP-IE (AP onset,
517 ($\chi^2 = 1.195$, df = 3, $p = 0.754$; 1st AP latency, $\chi^2 = 3.149$, df = 3, $p = 0.369$, Kruskal-Wallis test), suggesting
518 that the CA3 ensemble cells had already underwent LTP-IE *in vivo*. In contrast, ctxAB(++/2) cells were not
519 different from GFP(-) cells with regard to all aspects: G_{in}, AP onset time and AP latency before and after
520 somatic conditioning [baseline AP onset time, $p = 0.419$; AP latency, $p = 1.00$].

521

522 *PP-EPSP/PP-EPSC ratio is highly correlated with input conductance*

523 Next, we examined PP-EPSPs in CA3-PCs *ex vivo* from cfos-shEGFP mice that have experienced context A
524 or A/B as shown in Fig. 6A. Because LTP-IE enhances the excitability of distal apical dendrite rather than
525 PP-EPSC (Hyun et al., 2015), we measured the PP-EPSP and PP-EPSC in the same cells, and compared the
526 EPSP/EPSC ratio between different cell groups. The stimulation intensity was adjusted such that PP-EPSC
527 amplitudes are largely in the range of 10 to 20 pA and corresponding PP-EPSPs were measured in the
528 same cell. Similar to the distribution of G_{in} as a function of G/R ratio (Fig. 6Cd), the EPSP/EPSC ratio was
529 higher in ctxA60(+), ctx90(+), and ctxAB(+) cells than GFP(-) cells, and those of ctxAB(++) cells were
530 heterogenous (Fig. 7Aa). The plot of the baseline EPSP/EPSC ratio as a function of baseline G_{in} revealed
531 highly negative correlation of the baseline EPSP/EPSC ratio to the baseline G_{in} (Pearson's $r = 0.795$, $p <$
532 0.001, Pearson correlation test; Fig. 7Ab). Similar to the G_{in} ratio of ctxAB(++) cells (Fig. 6Cc), the
533 EPSP/EPSC ratios of those cells were split into two clusters. Because ctxAB(++) cells with low G_{in} exhibited
534 high EPSP/EPSC ratio and vice versa (Fig. 7Ab), ctxAB(++) cells exhibiting high EPSP/EPSC ratio were
535 regarded as ctxAB(++/1) cell, and the other subgroup as ctxAB(++/2) cell. Similar to G_{in}, EPSP/EPSC ratio
536 of shEGFP(+) cells were categorized two groups: low and high excitability groups, which are comprised of
537 GFP(-) and ctxAB(++/2) cells *vs*. ctxA60(+), ctxA90(+), ctxAB(+) and ctxAB(++/1) cells, repspectively ($F_{(5,33)}$
538 $= 24.864$, $p < 0.001$; one-way ANOVA and Tukey HSD). Fig. 7B shows representative traces for PP-EPSC
539 and PP-EPSP, and the time course for the EPSP/EPSC ratio changes before and after somatic conditioning
540 in five cell groups (the same colour codes as in *A*). Not only the baseline PP-EPSC amplitudes but also those
541 after somatic conditioning were not different between cell groups (Fig. 7Ba and Ca). However, the baseline
542 PP-EPSP amplitudes were significantly higher in the high excitability group than the low excitability group
543 [low vs. high excitability group, $F_{(5,33)} = 24.864$, $p < 0.001$; 1-way ANOVA and Tukey HSD; Fig. 7Bb and 7Cb].
544 For the cells of high excitability group, somatic conditioning did not further enhance the PP-EPSP while it
545 did in the cells of low excitability group (Fig. 7Bc and 7Cb). The baseline EPSP/EPSC ratios of cells in the
546 high excitability group were not different from post-SC EPSP/EPSC ratio measured in GFP(-) and
547 ctxAB(++/2) cells ($\chi^2 = 1.365$, df = 3, $p = 0.714$, Kruskal-Wallis test; Fig. 7Bc]. These notions are also evident
548 from the plot of individual cells on the plane of PP-EPSP vs. PP-EPSC amplitude in Fig. 7D. Finally, similar
549 to G_{in}, the baseline EPSP/EPSC ratio was closely correlated with inducibility of LTP-IE probed by
550 potentiation of EPSP/EPSC ratio (Fig. 7E). In this plot, cells were also classified into two groups by *k*-means
551 clustering. The shEGFP(+) cells except ctxAB(++/2) cells comprised a cluster distinct from GFP(-) cells,
552 supporting the notion that these cells have already undergone LTP-IE probably while the animal visited

553 context A or B (potentiation of ratio, t = -5.985, p < 0.001; Baseline ratio, t = 7.899, p < 0.001, *k*-means
554 clustering and independent t-test; Fig. 7E). The ctxAB(++/2) cells (n = 7) well overlapped with GFP(-) cells
555 (potentiation of EPSP/EPSC ratio, t = -0.171, p = 0.868; baseline ratio, t = 0.154, p = 0.881, independent t-
556 test; Fig. 7E). These results suggest that ctxAB(++/2) cells are not different from GFP(-) cells in distal
557 dendritic excitability, even though they are supposed to be recruited to ensembles A and B twice.

558

559 *Lack of LTP-IE in the ensemble CA3-PCs of ZnT3 hetero-knockout mice*

560 The results of the present study together with Eom et al. (2019) indicate that MF-induced Zn^{2+} signalling
561 inhibits protein tyrosine phosphatase, and thus widens the cytosolic [Ca^{2+}] window for LTP-IE induction of
562 and maintains LTP-IE in the normal redox state. We tested whether LTP-IE occurs *in vivo* when MF-induced
563 Zn^{2+} signalling is disrupted by hetero-insufficiency of ZnT3, a vesicular Zn^{2+} transporter. To this end, ZnT3
564 hetero-knockout(HT) x cfos-shEGFP hybrid mice (ZnT3HT/cfos-EGFP) were made by crossing ZnT3-
565 knockout (KO) mice with cfos-shEGFP mice. We confirmed that LTP-IE was induced by 20 Hz MF
566 stimulation but not by 50 Hz stimulation in CA3-PCs of ZnT3HT mice (n =5, t = -1.141, p = 0.318, paired t-
567 test; Fig. 8A), similar to those of ZnT3-KO mice (Eom et al, 2019). Next, we examined correlation of G_{in}
568 with G/R ratio in ZnT3HT/cfos-shEGFP mice which experienced context A and B as shown in Fig. 8B. Unlike
569 wildtype CA3-PCs, CA3-PCs of ZnT3HT/cfos-shEGFP mice exhibited high G_{in} regardless G/R ratio (Fig 8C
570 and Da). Moreover, 10 Hz somatic conditioning induced LTP-IE in high G/R ratio cells as well as GFP(-) cells
571 (Fig 8C and Db), indicating that induction and/or maintenance of LTP-IE is impaired in vivo in ZnT3-HT mice.
572 Given that dendritic Zn^{2+} transients in CA3-PCs were induced by MF inputs but not by PP or A/C inputs,
573 these results suggest that CA3-PCs that received high-frequency MF inputs undergo LTP-IE in vivo.

574

575 *Computational modelling of the association of two temporally separated events in the CA3 network*

576 To conceive possible roles of MF-induced LTP-IE and non-MF input-induced depotentiation in the CA3
577 network dynamics, we incorporated our findings into a CA3 recurrent network model. The assumptions
578 adopted for the model is based on the Hebb-Marr network (McNaughton & Morris, 1987) and the
579 computational theory of CA3 function (Lee & Kesner, 2004; Treves & Rolls, 1992), and are described in
580 detail in *Materials and Methods*.

To implement these LTP-IE-based learning rules, we constructed a computational model of recurrent network comprised of 1000 PCs and 200 interneurons (INs) *in silico*, which are numbered with indices from 1 to 1000 and 1001 and 1200, respectively. Fig. 9A and Fig. S5A show the schematic synaptic connections between PCs and INs, and the initial connectivity map of the model network, respectively. We assumed that PCs make excitatory synapses with each other with the probability of 10%. The synaptic weights between PCs were randomly set to a value between 0 and 0.35 nS. The spike properties of PCs and INs were assumed to follow a leaky integrate and fire model using parameter sets as described in Methods and Fig. S5.

We considered an animal which experiences a series of episodes, which present MF and PP afferent inputs to CA3-PCs carrying the information of *i*-th episode as *i*-th pattern (denoted as $\boldsymbol{P}_i$). The model network was trained by four patterns that arrive at the network in a sequence with different time intervals (0.8-1.2 s) as shown in Fig. 9Ba (We adopted here short time intervals to lessen computational time, but longer time intervals do not alter the main conclusion). Each input pattern is comprised of sparse non-overlapping MF and diffuse PP inputs (red and blue dots in Fig. 9Ba, respectively). The arrival of MF inputs in each pattern is confined in a subset of 200 PCs, which constitute an **M** subset, while PP inputs arrive over all the PCs in the network. We assumed that each PC receives different numbers of MF or PP inputs per a pattern, which are randomly given under a log-normal distribution (Ikegaya et al., 2013) (Fig. 9Ba and Fig. S5D). During the encoding phase, PP and A/C synapses of PCs undergo plastic changes under the spike timing dependent plasticity (STDP) rules. We assumed symmetric and asymmetric STDP curves for A/C and PP synapses, respectively (Mishra et al., 2016) (Fig. S5B).

Our results suggest that coincident increases in cytosolic $[Ca^{2+}]$ and $[Zn^{2+}]$ induce LTP-IE, while $[Ca^{2+}]$ increase alone reverses LTP-IE. In our simulation, the $[Ca^{2+}]$ and $[Zn^{2+}]$ thresholds required for triggering LTP-IE were set such that MF input-induced Ca^{2+} and Zn^{2+} transients cross the threshold in about 25% of PCs of an **M** subset during encoding phase. A subset of CA3-PCs that undergo LTP-IE during encoding of $\boldsymbol{P}_i$ will be denoted as $\mathbf{M}_i$*****. Exemplar traces for $[Ca^{2+}]_i$ and $[Zn^{2+}]_i$ simulated in an $\mathbf{M_1}$***** PC are shown in Fig. 9C. To simulate the time course of excitability change we defined an intrinsic excitability parameter, *IE*, which varies from 0 to 1. *IE* is equal to 0 when a cell is in a resting state, and it starts to increase toward one when both $[Ca^{2+}]_i$ and $[Zn^{2+}]_i$ co-incidentally surpass Ca^{2+} and Zn^{2+} thresholds (Caθ1 and Znθ, respectively). Once *IE* is increased by MF inputs, it stays high until a CaT occurs devoid of ZnT. Subsequently incoming PP inputs can induce APs independent of MF inputs in such primed PC. To simulate this, a transient current was injected upon arrival of PP inputs to a primed PC that has *IE* > 0.7 (Fig. S5)(Jahnke et al., 2015). The

612 PP input to a primed cell readily elicits APs in a postsynaptic PC resulting in a CaT devoid of Zn^{2+} signaling.
613 When the peak of a PP-induced CaT is higher than a given Ca^{2+} threshold (Caθ2), the *IE* returns to zero
614 (de-potentiation; Fig. 9C). Fig. 9Bb shows the simulation results for the firing of PCs in response to the
615 four sequentially incoming input patterns shown in Fig. 9Ba. The PP inputs of $\boldsymbol{P_2}$ readily elicit firings of the
616 $\mathbf{M_1}$***** PCs (subset of primed PCs in $\mathbf{M}_1$), and thus fire together with PCs of the $\mathbf{M_2}$ subset. These concomitant
617 firing of PCs in $\mathbf{M_1}$***** and $\mathbf{M_2}$ subsets allows recurrent synapses to be strengthened between the two
618 orthogonal ensembles. Fig. 9D shows a matrix of recurrent synaptic weights consequent to these auto-
619 and hetero-associative learning rules.
620 Next, we tested whether the recurrent network trained under these learning rules recalls the whole
621 sequence of memories from a partial cue of $\boldsymbol{P}_1$. We assumed no reduction in A/C synaptic weight during
622 recall, because recall occurs under the low cholinergic state such as quiet awake state or slow wave sleep.
623 To trigger pattern completion-based recall of the memory of $\boldsymbol{P}_1$, which is represented by $\mathbf{M_1}$, a burst of PP
624 inputs carrying a part of $\boldsymbol{P_1}$ (denoted as $\boldsymbol{p_1}$) was applied to the network (Fig. S5D). The synaptic weights of
625 the PP inputs of $\boldsymbol{p_1}$ have been already strengthened during encoding phase only in $\mathbf{M_1}$ PCs. The PP inputs
626 of $\boldsymbol{p_1}$ drive firing in a few $\mathbf{M_1}$ PCs (14 PCs in the example shown in Fig. 9E), which propagated through
627 already strengthened recurrent connections, resulting in pattern completion-based recall of $\mathbf{M_1}$ (Fig. 9E).
628 Meanwhile, the activation of PCs in $\mathbf{M_1}$* plays a role of partial cue to $\mathbf{M_2}$, and triggers the second pattern
629 completion-based recall of $\mathbf{M_2}$. In this way, the PP inputs carrying a partial cue of $\boldsymbol{P}_1$ trigger the recall of
630 whole sequence of memories that were hetero-associated during encoding phase (from $\mathbf{M_1}$ to $\mathbf{M_4}$). This
631 simulation implies that LTP-IE may allow the CA3 network to recall of memories of sequential events, even
632 if they are temporally separate.

633

634 *Summary for the ensemble dynamics in the CA3 network*

635 Based on our CA3 network model (see *Materials and Methods*), memories for two temporally separate
636 events can be associated in the CA3 model network via the following mechanism:

637 1. *CA3-PCs primed by $\boldsymbol{P_1}$ are readily fired by PP input alone during the encoding phase of $\boldsymbol{P_2}$*: We assumed
638 that a fraction of $\mathbf{M_1}$ PCs receives strong MF inputs during encoding phase of $\boldsymbol{P_1}$, and undergo LTP-IE,
639 resulting in enhanced E-S coupling of subsequently incoming PP inputs. These primed PCs of $\mathbf{M_1}$ subset
640 (denoted as $\mathbf{M_1}$***** PCs) are readily fired by PP inputs alone of the next pattern $\boldsymbol{P}_2$.

641 2. *Upon the arrival of* $\boldsymbol{P}_2$ *PP-LTP is induced not only in* $\boldsymbol{M_2}$ *PCs but also in* $\boldsymbol{M_1}$***** *PCs*: Sparse and decorrelated
642 MF inputs of $\boldsymbol{P}_2$ create an $\mathbf{M_2}$ subset orthogonal to the $\mathbf{M_1}$ subset. The orthogonality of $\mathbf{M_1}$ and $\mathbf{M_2}$ subsets
643 makes hetero-association of the two subsets unlikely when the two episodes occur in a temporally
644 discontiguous sequence. However, PP inputs of $\boldsymbol{P_2}$ to the $\mathbf{M_1}$* PCs readily elicit postsynaptic APs, which
645 facilitate LTP induction at PP synapses carrying $\boldsymbol{P}_2$. Therefore, the PP inputs of $\boldsymbol{P_2}$ induce LTP not only in
646 $\mathbf{M_2}$ but also in $\mathbf{M_1}$* PCs. Furthermore, the primed state is reversed (depotentiation) by burst firing
647 elicited by PP inputs as shown in Fig. 4. Thus, the $\mathbf{M_1}$* PCs do not fire any longer in response to PP inputs
648 in response to subsequent patterns.
649 3. *Recurrent connections are strengthened between PCs in* $\boldsymbol{M_2}$ *and* $\boldsymbol{M_1}$*: $\boldsymbol{P}_2$ elicits firing both of $\mathbf{M_2}$ PCs and
650 $\mathbf{M_1}$* PCs, and thus recurrent connections are strengthened not only between $\mathbf{M_2}$ PCs but also between
651 $\mathbf{M_2}$ and $\mathbf{M_1}$* PCs. Therefore, the $\mathbf{M_1}$* PCs play a key role in association between $\mathbf{M_1}$ and $\mathbf{M_2}$, the two
652 ensembles which encode $\boldsymbol{P}_1$ and $\boldsymbol{P}_2$, respectively.
653

654 ## Discussion

655 ### *Cellular signalling that de-potentiates LTP-IE*

656 We showed that non-MF inputs which evoke CaTs without Zn^{2+} signaling reverse the MF-induced LTP-IE
657 in CA3-PCs. Although both somatic- and MF-induced LTP-IE was long lasting under the conventional patch
658 clamp conditions (Hyun et al., 2015; Hyun et al., 2013), in the presence of GSH, LTP-IE was sustained only
659 upon MF conditioning but not upon somatic conditioning. Moreover, the MF-induced LTP-IE was
660 effectively terminated by non-MF inputs. How can the intrinsic excitability of CA3-PCs be reversibly
661 regulated in input-specific manners? Previous studies have showed that PTK downregulates Kv1.2-
662 mediated current (Hyun et al., 2013; Lev et al., 1995), whereas RPTPα upregulates it (Tsai et al., 1998).
663 Subsequent studies revealed that the activity of PTPs is reversibly suppressed by reactive oxygen species
664 (ROS) (Meng et al., 2002), suggesting that redox homeostasis is important for the balance between PTKs
665 and PTPs. We previously showed that CaTs in CA3-PCs activate not only PTK but also RPTPα (Eom et al.,
666 2019), supporting the previous findings that the CaTs activates PTPs and PTKs (Grishin et al., 2005; Hyun
667 et al., 2013). The loss of cytosolic GSH caused by whole-cell recording would bias the enzymes involved in
668 tyrosine phosphorylation toward PTK through oxidative inactivation of PTPs, resulting in prolonged
669 downregulation of Kv1.2 mediated by PTK. This idea explains the reason why the supplement of GSH
670 renders the somatic conditioning-induced potentiation of intrinsic excitability (PIE) short-lasting. In
671 contrast, MF-induced PIE was not affected by intracellular GSH probably because MF-induced ZnTs
672 prevented the Ca^{2+}-mediated activation of PTPs, resulting in prolonged PIE even without oxidative
673 inactivation of PTPs. Given that MF-induced Zn^{2+} signaling may be temporary, the MF-induced PIE can be
674 reversed by Ca^{2+}-induced activation of PTPs, which may be triggered later by non-MF synaptic inputs that
675 induce CaT without Zn^{2+} signaling.
676

677 ### *LTP-IE occurs in the CA3 ensemble cells*

678 The present study suggests that LTP-IE is de-potentiated not only by PP inputs probably during the
679 encoding phase (Fig. 4) but also without any episodic events within 3 hours (Fig. 5). A/C input strength is
680 critically modulated by acetylcholine (Ach) level. High Ach level in the hippocampus during awake and
681 active learning state enhances MF synapses and suppresses A/C synapses (Vogt & Regehr, 2001). When
682 Ach level is low during a retrieval or consummatory phase, the suppression of A/C synapses is relieved
683 resulting in spontaneous offline reactivation of neuronal ensembles, manifested as sharp wave ripples

684 (SWRs). Unlike PP-EPSPs, A/C-EPSPs are not enhanced by LTP-IE (Hyun et al., 2015). In the low cholinergic
685 state, however, A/C input-driven firings of CA3-PCs would be facilitated (Kowalski et al., 2016; Malezieux
686 et al., 2020), and may contribute to depotentiation of LTP-IE even if A/C inputs do not induce IEG
687 activation. This possibility may be responsible for depotentiation of LTP-IE while animals were kept in the
688 homecage. It remains to be tested whether the activation of non-MF synapses to CA3-PCs during low
689 cholinergic state de-potentiates LTP-IE.

690 Immediate early gene (IEG)-induced expression of fluorescence protein has been widely used for labeling
691 ensemble cells to investigate the recall of memory represented by them. To investigate whether LTP-IE is
692 reversed by the second activation of ensemble cells, it is essential to distinguish once- vs. twice-activated
693 ensemble cells in an animal that experienced two contexts within 2 hours because LTP-IE is spontaneously
694 reversed less than 3 hours (Fig. 5). No currently available labeling technique meets these requirements,
695 although techniques for labeling active population of neurons with high temporal precision has been
696 recently developed (Lee et al., 2017; Moeyaert et al., 2018). Thus, we compared the expression of c-fos
697 promoter-induced shEGFP expression level between cfos-shEGFP transgenic mice which were exposed a
698 novel context once and twice (denoted as ctxA and ctxAB mice). Because a subset of ensemble CA3-PCs
699 from the ctxAB mice expressed distinctly high level of shEGFP compared to those from the ctxA mice
700 observed by both confocal and epifluorescence microscopy (Fig. S4 and Fig. 6-7), we regarded such GFP(++)
701 subset as twice-activated ensemble cells. Nevertheless, it cannot be ruled out that it contains once-
702 activated ensemble cells.

703

704 *Why a subset of ctxAB(++) cells exhibit G_{in} similar to that of non-ensemble cells?*

705 CA3-PCs with distinctly high EGFP expression from ctxAB mice were comprised of mixed population in the
706 excitability (Fig. 6). Why ctxAB(++/2) cells exhibit the normal excitability despite that these cells may
707 participate in both ensembles encoding contexts A and B? There are two possibilities for the normal
708 excitability of ctxAB(++/2) cells. First, these cells may have never experienced LTP-IE. Alternatively, they
709 underwent LTP-IE in context A, and the LTP-IE is de-potentiated in context B. The first possibility is unlikely
710 because most CA3 ensemble cells of the animal that visited only context A exhibited high excitability
711 (ctxA60(+) and ctx90(+) cells). Previously we showed that MF inputs are privileged for the induction of
712 LTP-IE (Eom et al, 2019). Moreover, Figure 1 suggests that, even if the excitability would be enhanced by
713 non-MF inputs, the high excitability state cannot be sustained longer than 30 min under the physiological

714 redox conditions. Since we examined G_{in} at 60 min after the last visit, ctxAB(++) cells as well as ctxA60(+)
715 and ctxA90(+) cells may have received high frequency MF inputs while the animal visited context A,
716 assuming that ctxAB(++) are twice-activated ensemble cells. If the latter possibility is correct, the
717 mechanism underlying de-potentiation of LTP-IE can be explained by our findings that non-MF inputs
718 reversed the high excitability state of CA3-PCs induced by MF inputs that non-MF inputs reversed the high
719 excitability state of a CA3-PC induced by MF inputs (Fig. 2, 3 and 4). Moreover, CA3-PCs in the primed
720 state readily fire in response to subsequently arriving high frequency PP inputs, which also reverse the
721 high excitability state (Fig. 4). Given that ctxAB(++) cells are activated both in context A and B, their firing
722 in context B can be elicited not only by MF inputs but also by PP inputs alone as long as the LTP-IE is
723 maintained while the animal visited context B. Therefore, ctxAB(++) cells may be comprised of two groups:
724 CA3-PCs that received high frequency MF inputs in both contexts, and those received MF inputs in context
725 A and subsequently only PP inputs in context B. The latter group may undergo MF-induced LTP-IE in
726 context A and PP-induced depotentiation in context B, and thus eventually exhibit normal baseline G_{in},
727 because PP inputs can reverse the prior MF input-induced LTP-IE (Fig. 4).

728

729 *Implications of synaptic input-specific bidirectional regulation of intrinsic excitability*

730 The regulation of intrinsic excitability of CA3-PCs through a balance between PTKs and PTPs has important
731 implications in understanding the mechanisms by which information incoming through MFs and PP is
732 encoded in a subset of CA3-PCs during memory formation of sequential events. Our simulation results
733 imply that CA3-PCs primed by LTP-IE (**M*** subset) can play a key role in linking memories of temporally
734 spacced events under the framework of the Hebb-Marr network model. Hippocampal CA3 has been
735 implicated in memory of temporally discontiguous sequential events (Farovik et al., 2010). Previously, two
736 models proposed a possible mechanism for the association of memories of discontiguous events in a
737 recurrent network (Levy et al., 2005; Wallenstein et al., 1998). Both models assumed CA3-PCs which fire
738 in background (background cells) in addition to those encoding items or events presented in a sequence
739 (item cells). They proposed that repeated training may re-organize recurrent connections among
740 background cells and/or between background and item cells, and eventually bridge ensembles
741 representing two temporally discontiguous events. These models are critically different from the present
742 study in that 1) they are not constrained to the framework of Hebb-Marr model, and thus assumed that
743 CA3-PCs are readily fired by PP or A/C inputs alone during the learning phase; 2) the dependence of

synaptic potentiation on the time gap between pre- and postsynaptic firings is asymmetric, which is not supported by the recent finding (Mishra et al., 2016).

Recently, it has been demonstrated that two CA1 neuronal ensembles overlap even if each represents distinct contexts that an animal visited with a time gap up to 5 hours (Cai et al., 2016). The overlap of ensembles was proposed as a mechanism underlying memory link. Synaptic tagging and capture hypothesis and/or post-learning CREB-dependent modification of intrinsic excitability have been postulated as cellular mechanisms for the CA1 ensemble overlap (allocate-to-link hypothesis; (Kastellakis et al., 2016; Lisman et al., 2018; Silva et al., 2009). Similar to CA1, the post-learning CREB-expression may enhance intrinsic excitability of a CA3-PC subset after learning. Previous studies on the excitability of CREB-overexpressing cells indicate that CREB induces global excitability changes such as AP threshold, post-burst after-hyperpolarization and the spike numbers in response to a given current injection (Dong et al., 2006; Lopez de Armentia et al., 2007), implying that CREB-dependent metaplasticity is not input-specific, whereas MF-induced LTP-IE primes specifically PP synapses (Hyun et al., 2015).

Unlike CA1 network, CA3-PCs are extensively interconnected through recurrent synapses. The recurrent network subserves auto-associative learning through Hebbian plasticity between PCs within an ensemble. The number of PCs recruited to an ensemble is relevant to the stability of later memory retrieval and the capacity of memory storage in a recurrent network (Bennett et al., 1994). A large number of PCs in an ensemble would facilitate reliable retrieval of memory, but would lead to rapid depletion of memory storage capacity for future learning. Given that recurrent synapses are strengthened between cells within an ensemble, larger overlap between two ensembles would facilitate co-firing of the two neuronal subsets and disruption of pattern separation. Therefore, it is necessary to tightly regulate the overlapping fraction between two distinct ensembles particularly in order to maintain orthogonality between the ensembles in a recurrent network. We speculate that LTP-IE-based regulation of intrinsic plasticity of CA3-PCs may be appropriate for this purpose compared to the CREB-dependent excitability regulation, in that MF-induced LTP-IE specifically enhances feed-forward synaptic connections (via PP) without affecting feedback or recurrent synapses (Hyun et al., 2015). Moreover, the LTP-IE-based hetero-association of ensembles can prevent uncontrolled overlap between non-adjacent ensembles in a sequence (for example, link of $\mathbf{M_1}$ and $\mathbf{M_3}$), whereas CREB-dependent memory link is expected to facilitate overlap of ensembles encoding events regardless of their position in a sequence as long as sequential events occur in 6 hours, during which phosphorylated CREB level is kept high (Rashid et al., 2016). It remains to be

774 elucidated how LTP-IE and CREB-dependent regulations of intrinsic excitability contribute in concert to
775 memory allocation and link in the CA3 network.
776

777 Conclusions

778 MF- and PP-induced bi-directional regulation of CA3-PC excitability occurs in vivo, and may play a key role
779 in linking two orthogonal ensembles that encode two events adjacent in a sequence even if they are
780 temporally separated with the overlap between the two ensembles tightly regulated.

781

782 ## Supplemental Results

783 ### *Determination of PP-LTP threshold before and after somatic or MF conditioning*

784 We examined the role of LTP-IE in metaplastic regulation of PP inputs using GSH-free pipette solution (Fig.
785 S3). To this end, we first determined the threshold of stimulation strength for PP-LTP induction adopting
786 the same HFS protocol as (McMahon & Barrionuevo, 2002), which consists of 10 bursts repeated every 10
787 s with each burst being composed of 20 pulses at 100 Hz (PP-HFS, Fig. S3Aa and S4Ba). Testing PP
788 stimulation of different intensities, we found that PP-LTP requires strong PP inputs sufficient to elicit
789 somatic APs during the LTP induction (Fig. S3A and S4B). Because PP-EPSPs are affected by dendritic
790 excitability, PP stimulation intensity was quantified as the baseline PP-EPSC amplitude. The potentiation
791 ratio was measured as the baseline-normalized PP-EPSC amplitudes 30 min after PP-HFS, and plotted as
792 a function of corresponding PP stimulation intensity (quantified as baseline EPSC amplitudes) in Fig. S3C.
793 We fitted a logistic function to this relationship. We regarded more than 50% increase of PP-EPSC
794 amplitude at 30 min of PP-HFS compared to the baseline value as successful PP-LTP induction (Chen et al.,
795 2006). The x-value of the fitted function at 150 was read as 12.55 pA. The PP-HFS with baseline EPSC <
796 12.55 pA did not induce PP-LTP (Fig. S3Ab), whereas PP-HFS with EPSC > 12.55 pA did (Fig. S3Bb). Next,
797 we tested whether weak PP-HFS (baseline PP-EPSC < 12.55 pA) which does not induce PP-LTP in a naïve
798 PC, can trigger PP-LTP in the CA3-PCs that have undergone MF or somatic conditioning. Despite of the
799 weak stimulation intensity, PP-HFS readily elicited APs in the CA3-PCs, which underwent MF or somatic
800 conditioning, indicative of E-S potentiation (Fig. S3Da, *upper* and *lower*, respectively). Consistent with
801 (Hyun et al., 2015), neither MF conditioning nor somatic conditioning (arrowhead, Fig. S3Db) altered PP-
802 EPSCs (Fig. S3Dc, Ea, Eb), but both of them enhanced PP-EPSPs that were measured 6 min after the
803 conditioning (Fig. S3Dc, Ec, Ed). Distinct from the naïve CA3-PCs (Fig. S3Aa), weak PP-HFS readily induced
804 PP-LTP in conditioned CA3-PCs (Fig. S3Db, Ea, Eb). The PP-EPSPs in the conditioned CA3-PCs were also
805 enhanced after the weak PP-HFS (Fig. S3Ec, Ed). For the conditioned CA3-PCs, the potentiation ratios are
806 plotted as a function of baseline EPSC amplitudes in Fig. S3C, showing that the threshold for PP-LTP
807 induction is lowered in the CA3-PCs compared to naïve CA3-PCs.

808

809 ## Figure Legends

810 *Fig. 1*

811 **Fig. 1 Differential effects of intracellular GSH on somatic and MF conditioning-induced LTP-IE. Aa** and
812 **Ba.** Mean baseline-normalized input conductance (G_{in}) and PP-EPSP amplitude of CA3-PCs before and
813 after MF (red) or somatic (black) conditioning (arrowheads). Right two insets of Aa, Voltage responses to
814 subthreshold current injection for measuring G_{in} before and after MF (middle) and somatic (right)
815 conditioning. Insets of Ba, PP-EPSCs (upper) and PP-EPSPs (lower) before and after MF (left) or somatic
816 (right) conditioning. The time points of recording are indicated by asterisks (same color codes). **Ab-Ac.**
817 Summary for G_{in} at baseline, 10 min and 30 min after the MF (*Ab*) or somatic (*Ac*) stimulation. For MF
818 conditioning, 0 vs. 10 min, $p < 0.001$; 0 vs. 30 min, $p < 0.001$; 10 vs. 30 min, $p = 0.190$ (GLM and simple
819 effect analysis). For somatic conditioning, 0 vs. 10 min, $p < 0.001$; 0 vs 30 min, $p = 0.533$; 10 vs. 30 min: p
820 < 0.001 (GLM and simple effect analysis). Here, the baseline values are denoted as 0. **Ad-Ae.** Voltage
821 responses to ramp current injection measured before (black), 10 min (blue) and 30 min (red) after MF (*Ad*)
822 and somatic (*Ae*) conditioning. **Af-Ag.** Mean latency of first AP before, and 10 min and 30 min after the
823 MF (*Af*) or somatic (*Ag*) conditioning (For MF, 0 vs. 10 min, $p < 0.001$; 0 vs. 30 min, $p < 0.001$; 10 vs. 30
824 min, $p = 0.964$; For somatic, 0 vs. 10 min, $p < 0.001$; 0 vs. 30 min, $p = 0.054$; 10 vs. 30 min, $p < 0.001$; GLM
825 and simple effect analysis). **Bb-Be.** Mean PP-EPSP (Bb-Bc) and PP-EPSC (Bd-Be) amplitudes at baseline, 3
826 min and 30 min after MF (Bb, Bd) or somatic (Bc, Be) conditioning. For EPSP/MF conditioning, 0 vs. 10 min,
827 $p < 0.001$; 0 vs. 30 min, $p < 0.001$; 10 vs. 30 min: $p = 0.779$. For EPSP/somatic conditioning, 0 vs. 10 min, p
828 < 0.001, 0 vs. 30 min, $p = 0.481$; 10 vs. 30 min, $p < 0.001$ (GLM and simple effect analysis).

829 *Fig. 2*

830 **Fig. 2, Restoration of MF-induced potentiation of PP-fEPSPs by A/C stimulation. Aa.** IR-DIC images for
831 extracellular recording setup. The recording electrode was placed on the CA3 SLM. Three stimulating
832 electrodes were placed on the SLM of CA1 and subiculum border, granule cell layer of DG, and alveus of
833 CA3 to stimulated PP, MF, and A/C fibers, respectively. The silhouette of the each glass electrode is
834 indicated by a black solid line. **Ab.** Upper, Representative traces of fEPSPs evoked by paired pulse
835 stimulation of PP (PP-fEPSPs, 100 ms interval) with gradually increasing intensity ranging 10 to 70 V.
836 Middle, MF-evoked fEPSP. Lower, A/C-evoked fEPSP trace. The same color codes were used as in Aa. **Ac-**
837 **Ad.** Mean peak amplitude (Ac) and initial slope of PP-fEPSP (Ad) as a function of stimulation intensity. **Ba.**
838 Bath application of DCG-IV attenuated the PP-fEPSP amplitudes ($n = 5$, $t = 5.075$, $p = 0.007$; paired t-test).

839 **Bb.** PP-fEPSP latency was not affected by stimulus intensity (linear regression slope, t = -0.02, p = 0.98, n
840 = 5). **Bc.** IR-DIC images for whole-cell patch pipette on the CA3-PC and the glass electrode on the alveus
841 of CA3 for stimulation of A/C synapses. Yellow bars in *Aa* and *Bc*, 500 µm. **Bd.** Voltage response of the
842 CA3-PC to A/C stimulation recorded using whole-cell patch techniques before (red) and after (black) bath
843 application of CNQX. Inset, the same EPSPs evoked by first a few stimuli in an expanded scale. Scale bars,
844 100 ms and 10 mV. **Ca.** Peak amplitudes of 1st PP-fEPSP before and after MF conditioning (blue arrowhead)
845 and A/C conditioning (red arrowhead at 40 min). The PP-fEPSPs increased and reached a plateau 5 min
846 after MF conditioning. The PP-fEPSP stayed increased up to 40 min, and was restored to the baseline by
847 A/C conditioning. **Cb.** PP-fEPSP traces before (black; -15 min), and after MF conditioning (blue, +40 min)
848 and after A/C conditioning (red, +80 min). Lower, the first fEPSPs in expanded time scale (gray box). The
849 same color codes as the dots in Ca. **Cc.** Summary for the peak amplitudes of PP-fEPSPs before and after
850 MF (40 min) and A/C conditioning (80 min) ($F_{(2,10)}$ = 17.66, p = 0.005; baseline vs. 40 min, p = 0.002;
851 baseline vs. 80 min, p = 0.672; 40 vs. 80 min, p = 0.007; n = 6, RM-ANOVA and simple effect analysis). **Da.**
852 Neither the initial slope of first PP-fEPSP (black; $F_{(2,10)}$ = 0.174, p = 0.842) nor paired pulse ratio (PPR, light
853 red; $F_{(2,10)}$ = 0.057, p = 0.944, RM-ANOVA and simple effect analysis) measured from the peak amplitudes
854 of 1st and 2nd PP-fEPSPs were affected by the MF and A/C conditioning. **Db.** Summary for the initial slope
855 of PP-fEPSPs at the baseline, after MF conditioning and after A/C conditioning.

856 *Fig. 3*

857 **Fig. 3 Depotentiation of MF-induced LTP-IE can be induced by somatic or A/C synaptic stimulation, and**
858 **is hindered by Zn^{2+}. Aa-Ac**. Baseline- normalized G_{in} (filled circles) changes caused by MF conditioning at
859 0 min (blue arrowhead) and by somatic AP bursts at 15 min (red arrowhead) evoked by A/C stimulation
860 (*Aa*) or direct somatic current injection of ten (*Ab*) or two (*Ac*) pulses at 100 Hz. For A/C stimulation (*Aa*),
861 0 vs. 15 min, p < 0.001; 0 vs. 30 min, p = 0.945; 15 vs. 30 min, p < 0.001 (n = 7, GLM and simple effect
862 analysis). For somatic AP bursts (*Ab*), 0 vs. 15 min, p < 0.001; 0 vs. 30 min, p = 0.936; 15 vs. 30 min, p <
863 0.001 (n = 7, GLM and simple effect analysis). For two AP simulation (*Ac*), 0 vs. 15 min, p < 0.001; 0 vs. 30
864 min, p = 0.439; 15 vs. 30 min, p < 0.001 (n = 7, GLM and simple effect analysis). The MF-induced decrease
865 of G_{in} in the absence of intracellular GSH is reproduced from (Eom et al., 2019) for comparison (*gray*
866 *symbols*). For A/C synaptic activation, CA3 alveus was stimulated at 20 Hz for 0.5 s (A/C conditioning, Aa).
867 *Left inset*, Voltage response to MF conditioning. Middle inset, AP bursts induced by A/C conditioning (Aa)
868 or somatic current injection (Ab and Ac). *Right inset*, Representative voltage responses to somatic
869 subthreshold current injection (+10 and -30 pA) for measuring G_{in} at the time indicated by black (baseline),

870 blue (at 14 min), and red (at 29 min) asterisks. The same color codes were used for the asterisks and traces.
871 **Ad.** Summary for normalized G_{in} at the baseline, 15 min after MF conditioning, 15 min after the
872 depotentiation (time: $F_{(2,18)} = 162.345$, $p < 0.001$, stimuli: $F_{(2,18)} = 1.392$, $p = 0.274$, stimuli × time: $F_{(2,18)} =$
873 1.66, $p = 0.218$; GLM and simple effect analysis). **Ba-c.** Same as Aa-Ac but peak amplitudes of PP-EPSP
874 were monitored instead of G_{in}. For alveus stimulation (*Ba*), 0 vs. 15 min: $p = 0.012$; 0 vs. 30 min, $p = 0.818$,
875 15 vs. 30 min, $p = 0.011$ (n = 7, GLM and simple effect analysis). For 10 somatic APs (*Bb*), 0 vs. 15 min, $p =$
876 0.012; 0 vs. 30 min, $p = 0.848$; 15 vs. 30 min, $p = 0.011$ (n = 7, GLM and simple effect analysis). For 2 APs
877 (*Bc*), 0 vs. 15 min, $p = 0.006$; 0 vs. 30 min, $p = 0.801$; 15 vs. 30 min, $p = 0.004$ (n = 7, GLM and simple effect
878 analysis). *Gray symbols*, PP-EPSP amplitudes measured without intracellular GSH, which is reproduced
879 from (Eom et al., 2019) for comparison. *Blue arrowheads*, MF conditioning at 0 min. *Read arrowheads*,
880 second conditioning by CA3 alveus stimulation (*Ba*) or somatic injection of current pulses (*Bb* and *Bc*) at
881 15 min. *Insets*, Representative traces for PP-EPSPs recorded at time points indicated by asterisks with the
882 same color codes. **Bd**. Summary for the PP-EPSP amplitudes at baseline, 15 min after MF conditioning, 15
883 min after the second conditioning (time: $F_{(2,18)} = 71.199$, $p < 0.001$, stimuli: $F_{(2,18)} = 1.392$, $p = 0.274$, stimuli
884 × time: $F_{(2,18)} = 0.822$, $p = 0.520$; GLM and simple effect analysis). **Ca.** Time course of normalized G_{in} changes
885 (filled circles) caused by MF conditioning (20 Hz for 2 s) at 0 min (blue arrowhead) and subsequent somatic
886 100 Hz AP bursts for 0.1 s at 15 min (red arrowhead). For comparison, MF-induced decrease of G_{in}
887 measured in the absence of intracellular GSH is reproduced from previous study (Eom et al., 2019) (gray
888 symbols). $ZnCl_2$ was bath-applied 10 min after MF conditioning. Note that somatic AP bursts did not trigger
889 depotentiation of MF-induced LTP-IE in the presence of 100 nM $ZnCl_2$. (15 min vs. 30 min, $p = 1.00$; simple
890 effect analysis). **Cb.** Representative voltage traces in response to subthreshold current (+10 and -30 pA)
891 for measuring G_{in}. Voltage responses were measured before and c.a. 15 min after MF conditioning, and
892 c.a. 15 min after somatic AP bursts (indicated by black, blue and red asterisks in Aa, respectively). **Cc.**
893 Summary for the mean G_{in} at baseline, 15 min after MF conditioning, and 15 min after 100 Hz AP bursts
894 ($F_{(1,4)} = 16.109$, $p = 0.016$, RM-ANOVA; 0 vs. 15 min, $p = 0.007$; 0 vs. 30 min, $p = 0.002$; 15 vs. 30 min, $p =$
895 1.00; n = 5, GLM and simple effect analysis).

896 *Fig. 4*

897 **Fig. 4, MF-induced LTP-IE is terminated after homosynaptic PP-LTP.** WCRs of CA3-PCs was done using
898 GSH-containing pipette solution. **Aa.** Baseline-normalized amplitudes of PP-EPSPs were increased by MF
899 conditioning (20 Hz MF stimulation for 2 s, blue arrow) and further by PP-HFS with weak stimulation
900 intensity (red arrow). Insets, Representative traces of PP-EPSPs (upper) and PP-EPSCs (lower) and before

901 (black), after MF conditioning (blue), and after PP-HFS (red). The recording time points are indicated by
902 numbers in the main graph. **Ab.** Representative traces for voltage response to MF conditioning. **Ac.**
903 Voltage response to weak PP-HFS (10 bursts every 10 s, 20 pulses at 100 Hz per a burst; baseline EPSC <
904 12.55 pA). Inset, gray boxed region in an expanded time scale. **Ba.** Baseline-normalized G_{in} was decreased
905 by MF conditioning (blue arrow) and restored by PP-HFS (red arrow). G_{in} was monitored in the same cells
906 as in Aa ($F_{(1,4)} = 24.064$, $p < 0.001$; RM-ANOVA). **Bb**. *Upper*, Representative voltage responses to somatic
907 current injection of +10 and -30 pA at baseline (black), after MF conditioning (blue), and after PP-HFS (red).
908 *Lower*, Mean G_{in} at baseline, 6 min after MF conditioning, and 25 min after PP-HFS. Baseline vs. post-MF
909 conditioning, $p < 0.001$; baseline vs post-PPHFS, $p = 1.00$; post-cond. vs post-PPHFS, $p < 0.001$ (n = 7, GLM
910 and simple effect analysis). **Ca.** Summary for the mean amplitudes of PP-EPSPs (left, $F_{(1,4)} = 138.09$, $p <$
911 0.001; RM-ANOVA) and PP-EPSCs (right, $F_{(1,4)} = 35.751$, $p < 0.001$; RM-ANOVA) at baseline, after MF
912 conditioning, and after PP-HFS. For EPSP, baseline vs. post-MF cond., $p < 0.001$; baseline vs. post-PPHFS,
913 $p < 0.001$; post-MF cond. vs. post-PPHFS, $p < 0.001$; (n = 7, GLM and simple effect analysis). For EPSCs,
914 baseline vs. post-MF cond., $p = 0.647$; baseline vs. post-PPHFS, $p < 0.001$; post-MF cond. vs post-PPHFS, p
915 < 0.001 (n = 7, GLM and simple effect analysis); **Cb.** Scatterplot for PP-EPSP vs. PP-EPSC measured in the
916 same CA3-PCs at baseline (black), after MF conditioning (blue), and after PP-HFS (red). Baseline vs. post-
917 cond., $p < 0.001$; baseline vs post-HFS, $p = 1.00$; post-cond. vs post-HFS, $p < 0.001$; (n = 7, GLM and simple
918 effect analysis).

919 *Fig. 5*

920 Fig. 5, **The LTP-IE of CA3-PC did not last longer than 3 hours in vivo. Aa.** Schematic timeline of the
921 experimental procedure. Doxycycline was administrated via intraperitoneal route to prevent further
922 expression of GFP after visiting context A. Animals were sacrificed to prepare hippocampal slices after 1
923 hr, 1.5 hrs, and 3 hrs. **Ac-Ad.** IR-DIC image (*Ab*) and fluorescence image excited at 488 nm for GFP(+) CA3-
924 PCs (*Ac*: immediately after making whole-cell configuration; *Ad*: 30 min after whole-cell configuration.
925 Note that diffusion of GFP to the whole cell pipette in *Ad*). Scalebar, 30 µm. **B.** Baseline G_{in} as a function
926 of GFP fluorescence intensity (F_{GFP}). Most GFP(-) cells ($F_{GFP} = 3.38 \pm 0.30$ a.u.) showed high baseline G_{in}
927 [denoted as GFP(-/high) cells]. Some of GFP(-) cells (3.97 ± 0.47 a.u.), however, showed lower baseline G_{in}
928 [denoted as GFP(-/low) cells]. GFP(+) cells after 1 hr (27.68 ± 1.11 a.u.) and 1.5 hr (28.92 ± 4.16 a.u) showed
929 lower G_{in}. In contrast, GFP(+) cells after 3 hr (25.72 ± 3.63 a.u.) showed high G_{in} similar to GFP(-/high) cells.
930 **Ca.** Time course of G_{in} before and after somatic conditioning (indicated as blue arrowhead). Time points
931 at which G_{in} was measured for comparison between cell groups and the representative traces are shown

932 in *Cb* are indicated as black and red arrowheads (before and 30 min after somatic conditioning,
933 respectively). **Cb-Cc.** Representative voltage traces for different cell groups (same color code as *B* and *Ca*).
934 Traces for baseline G_{in} [GFP(-/high), 6.25 ± 0.26 nS (n = 8); GFP(+) at 1 hr, 4.68 ± 0.33 nS (n = 8); GFP(+) at
935 1.5 hr, 4.48 ± 0.33 nS (n = 5); GFP(+) at 3 hr, 6.59 ± 0.28 nS, $p < 0.001$ (n = 7)] were indicated as gray color.
936 **Cc**, Summary of G_{in} before (gray) and after (red) somatic conditioning (time, $F_{(1,24)} = 66.042$; fluorescence,
937 $F_{(3,24)} = 3.705$, $p = 0.025$; time x fluorescence, $F_{(3,24)} = 25.712$, $p < 0.001$, RM-ANOVA; For 1 hr, baseline vs.
938 post-SC, $p = 0.837$; For 1.5 hr, baseline vs. post-SC, $p = 0.554$; GLM and simple effect analysis).

939 *Fig. 6*

940 **Fig. 6**, **LTP-IE occurs in CA3 ensemble cells and may be reversed in part of twice-activated ensemble cells**.
941 **Aa.** Timeline of experimental procedures. *Upper*: Mice were subject to CFC in context A for 5 min, and
942 kept in homecage for 1 hr or 1.5 hr before ex vivo study (ctxA60 and ctxA90 mice). **Ab**. Mice additionally
943 visited context B 25 min after CFC, and then were kept in homecage (ctxAB mice). **Ba-d.** Fluorescence
944 images of two AF594-loaded CA3-PCs with low (Ba-b) and high (Bc-d) G/R ratios. **Be.** Summary for G/R
945 ratios. **Ca.** Time course of G_{in} changes in response to somatic conditioning. *Inset*, voltage response to 10
946 Hz somatic conditioning for 2 s (blue arrowhead). Small arrowheads indicate the time at which
947 representative traces shown in *Cb* and *Cc* were recorded. **Cb.** Representative traces for voltage responses
948 to -30 pA and +10 pA current steps in GFP(-), ctxA60(+), ctxA90(+), and ctxAB(+) cells. Traces before
949 conditioning are depicted in gray color, and those after somatic conditioning are in the same color codes
950 as in *Ca*. **Cc.** *Upper*, Representative voltage traces for G_{in} in ctxAB(++/1) and ctxAB(++/2) cells. *Lower*:
951 ctxAB(++) cells were clustered into two groups based on baseline G_{in} and G_{in} ratios before and after
952 somatic conditioning using k-means analysis. There was a significant difference between CtxAB(++/1) and
953 CtxAB(++/2) groups, and the centroids of two cell groups were depicted as cross symbols. **Cd-Ce.** Baseline
954 G_{in} (*Cd*) and G_{in} ratio (*Ce*) as a function of green-to-red fluorescence ratio (G/R ratio). The same color codes
955 used in *Ca-Ce*. **Da-b.** Representative traces for single AP evoked by short current injection and mean AP
956 onset time before and after somatic conditioning (condition, $F_{(5,27)} = 2.465$, $p = 0.058$; time, $F_{(1,27)} = 8.011$,
957 $p = 0.009$; condition x time: $F_{(5,27)} = 7.633$, $p < 0.001$; GLM and simple effect analysis). **Dc-d.** Representative
958 traces for first AP latency by ramp current injection and summary for change of first AP latency (condition,
959 $F_{(5,27)} = 3.044$, $p = 0.026$; time, $F_{(1,27)} = 11.951$, $p = 0.002$; condition x time, $F_{(5,27)} = 4.570$, $p = 0.004$). AP
960 onset time compared to GFP(-) cells, ctxA60(+), $p < 0.001$; ctxA90(+), $p < 0.001$; ctxAB(+), $p < 0.001$. For
961 first AP latency, ctxA60(+), $p < 0.001$; ctxA90(+), $p < 0.001$; ctxAB(+), $p < 0.001$.

962 *Fig. 7*

963 *Fig. 7,* Depotentiation of PP-EPSPs in twice-activated ensemble cells. **Aa.** Baseline EPSP/EPSC ratio as a
964 function of G/R fluorescence ratio. **Ab.** Potentiation of EPSP/EPSC ratio (ordinate) is closely correlated
965 with baseline G_{in} (abscissa). Color codes for GFP(-), gray; ctxA60(+), blue; ctxA90(+), green; ctxAB(+),
966 orange; ctxAB(++/1), violet; ctxAB(++/2), red. **Ba-b.** Representative traces for PP-EPSCs (*a*) and EPSPs (b)
967 before (gray) and after (colored) somatic conditioning. The same color codes as in *A*. **Bc.** Time courses of
968 PP-EPSP/EPSC ratio changes caused by somatic conditioning (large blue arrowhead at 0 min). *Inset*, AP
969 train induced by the somatic conditioning. Representative traces shown in a-b were recorded at time
970 points indicated by small arrowheads (black, baseline; red, 25 min). The same color codes as in *A*
971 (condition: $F_{(5,33)} = 6.657$, $p < 0.001$; time: $F_{(1,33)} = 20.375$, $p < 0.001$; condition x time: $F_{(5,33)} = 8.813$, $p <$
972 0.001; GLM and simple effect analysis). **C.** Summary for PP-EPSC (*a*) and EPSP (*b*) amplitudes before (gray)
973 and after (red) somatic conditioning. For EPSC, conditioning, $F_{(5,33)} = 0.406$, $p = 0.841$; time, $F_{(1,33)} = 0.130$,
974 $p = 0.720$; condition × time, $F_{(5,33)} = 0.891$, $p = 0.498$. For EPSP, conditioning, $F_{(5,33)} = 2.385$, $p = 0.059$; time,
975 $F_{(1,33)} = 21.676$, $p < 0.001$; condition × time, $F_{(5,33)} = 13.016$, $p < 0.001$; RM-ANOVA. For pre- vs post-SC
976 EPSPs (*Cb*), ctxA60(+), $p = 0.33$; ctxA90(+), $p = 0.160$; ctxAB(+), $p = 0.811$; ctxAB(++/1), $p = 0.368$;
977 ctxAB(++/2), $p < 0.001$; GFP(-), $p < 0.001$. **D.** PP-EPSP amplitude as a function of PP-EPSC of each CA3-PC.
978 The EPSP/EPSC ratio of CA3-PCs were categorized into two groups: high and low slope groups ($F_{(6,39)} =$
979 17.181, $p < 0.001$, 1-way ANOVA and Tukey HSD). Note that the post-SC EPSC/EPSC ratio of GFP(-) cells
980 belonged to the high slope group. **E**. Somatic conditioning-induced potentiation of EPSP/EPSC ratio as a
981 function of its baseline value. CA3-PCs were classified using k-mean analysis. There was a significant
982 difference between ctxAB(GFP++/1) and ctxAB(GFP++/2) groups. The same color codes as in *A*.

983 *Fig. 8.*

984 **Fig. 8, LTP-IE does not occur in CA3 ensemble cells of ZnT3 hetero-knockout mice**. **Aa.** G_{in} changes before
985 and after 50 Hz MF stimulation for 1 s in CA3-PCs of ZnT3HT mice (open symbols). The G_{in} changes induced
986 by 20 Hz 2 s MF (pink) and 50 Hz 1s MF stimulation (light blue) were reproduced from our previous study
987 (Eom et al. 2019). **Ab.** *Upper*: Representative traces for G_{in} before (black) and 25 min after MF conditioning
988 (upper) in CA3-PCs of ZnT3HT mice. *Lower*: Summary for G_{in} before and after 50 Hz MF conditioning in
989 CA3-PCs from ZnT3HT mice ($n = 5$, $t = -1.141$, $p = 0.318$, paired t-test). **B.** Timeline of experimental
990 procedure. **Ca.** G_{in} before and after 10 Hz 2 s somatic conditioning in CA3-PCs of ZnT3-HT/cfos-shEGFP
991 mice (black),. G_{in} before and after somatic conditioning in other groups of CA3-PCs were reproduced from

992 previous figure (Fig. 6, the same but pale colour codes). **Cb.** Representative traces for G_{in} before (black)
993 and 25 min after conditioning (*upper*) and summary of G_{in} before and after somatic conditioning in CA3-
994 PCs from ZnT3HT/cfos-shEGFP mice (n = 6, t = 7.675, p = 0.001, paired t-test). **Da-b.** Baseline G_{in} (*Ca*) and
995 post/pre-conditioning G_{in} ratio (*Cb*) as a function of G/R ratio in CA3-PCs of ZnT3-HT/cfos-shEGFP mice
996 (black). Colored symbols are reproduced from Fig. 6 with pale color.

997 *Fig. 9*

998 **Fig. 9 Input-specific bi-directional regulation of intrinsic excitability may contribute to sequential**
999 **memories. A.** Schematic illustration of CA3 network model comprised of pyramidal cells (PCs, black
1000 triangles) and an inhibitory interneuron (IN, green circle). **Ba.** Input patterns via MF (red dots) and PP (blue
1001 dots) during encoding phase. Inset, broken boxed region in an expanded scale. **Bb**. Raster plot of network
1002 responses to the input patterns shown in Ba. The distributions for the number of MF and PP inputs per a
1003 pattern are shown in Fig. S5D. The cell indices of 1 to 1000 are PCs, and the rest cell indices (1001 ~ 1200)
1004 are INs. **C,** Ca^{2+} (blue) and Zn^{2+} (red) transients in a PC in the $\mathbf{M_1}$ subset (cell id = 96) during the encoding
1005 phase. The timings of input pattern arrival are indicated by arrows below the abscissa. The intrinsic
1006 excitability index (IE, green broken line) starts to increase when both [Ca^{2+}] and [Zn^{2+}] are higher than their
1007 thresholds (Caθ1 = 1.5 a.u.; Znθ = 3 a.u.). When IE > 0.7, the arrival of subsequent PP inputs elicits a CaT
1008 devoid of Zn^{2+} signaling. When CaTs is higher than Caθ2 (= 0.9 a.u.) without Zn^{2+} signal, the IE returns to
1009 the baseline. Afterwards, this PC does not fire any longer in response to PP inputs alone. Note that the
1010 kinetics of Ca^{2+}, Zn^{2+} and IE were assumed faster than real values for the sake of reducing computing time
1011 (decay τ for CaT and ZnT = 150 and 300 ms, respectively; rise and decay τ for IE = 150 and 50 ms,
1012 respectively). **D.** Part of matrix of A/C synaptic weights (boxed in the Inset) resulting from training the
1013 recurrent network using a series of 4 patterns shown in Ba. Rows and columns represent indices of post-
1014 and pre-synaptic CA3-PCs, respectively. Synaptic weights are color-coded as shown on the right bar. Note
1015 that sparse potentiation of synaptic weights between $\mathbf{M_1}$ (cell index, 1-200) and $\mathbf{M_2}$ (cell index, 201-400)
1016 but not between $\mathbf{M_1}$ and $\mathbf{M_3}$ (cell index, 401-600). **E**, *Left*, Raster plot of network responses to the PP inputs
1017 shown in Fig. S5E. Note that most PP inputs are terminated in 30 ms (Fig. S5E), but the complete recall of
1018 $\mathbf{M_1}$ is accomplished by recurrent connections that have been strengthened during encoding phase. In turn,
1019 hetero-association between $\mathbf{M_1}$ and $\mathbf{M_2}$ that occurred during encoding phase allows subsequent activation
1020 of $\mathbf{M_2}$, and so on. Right, cumulative fraction of activated PCs in each ensemble.

1021 Supplementary Figure Legends

1022 *Fig. S1*

1023 **Fig. S1 Intracellular signaling cascade that mediates MF conditioning-induced downregulation of Kv1.2**
1024 **in CA3-PCs based on our previous studies (Hyun et al., 2013, 2015; Eom et al. 2019)**. (1) High frequency
1025 MF input elicits back-propagating APs (bAPs), which induce dendritic Ca^{2+} signaling through L-type voltage-
1026 dependent Ca^{2+} channels (VDCC). (2) The dendritic Ca^{2+} signaling activates protein tyrosine kinase (PTK),
1027 which induces endocytosis of Kv1.2 at distal apical dendrites. This downregulation of Kv1.2 underlies LTP-
1028 IE. (3) The dendritic Ca2+ signaling activates not only PTK but also receptor protein tyrosine phosphatase
1029 alpha (RPTPα), which antagonizes the PTK-dependent downregulation of Kv1.2. Thus, dendritic Ca^{2+}
1030 signaling alone caused by bAPs upon somatic current injection induces LTP-IE only in a narrow range of
1031 $[Ca^{2+}]i$ (c.a. 340-380 nM, Eom et al., 2019). (4) High frequency MF input, however, induces intracellular
1032 Zn^{2+} signaling together with bAP-mediated Ca^{2+}-signaling in postsynaptic CA3-PCs. The Zn2+ signaling
1033 inhibits RPTPα, and thus disinhibits the action of PTK leading to facilitation of LTP-IE.

1034

1035 *Fig. S2*

1036 **Fig. S2**. **Test for stability of whole-cell patch recordings in the presence of 5 mM GSH in the pipette**
1037 **solution. Aa.** Time course for baseline-normalized input conductance (G_{in}) of CA3-PCs. Inset,
1038 Representative traces for measuring G_{in} at the time indicated by arrowheads (black, 5 min; red, 45 min).
1039 **Ab.** Summary for G_{in} of CA3-PCs. Reduced glutathione (GSH) in the patch pipette solution did not change
1040 G_{in} of CA3-PCs over time (3.72 ± 0.42 nS to 3.87 ± 0.35 nS, n = 5, t = 0.223 p = 0.834, paired t-test). **Ba.**
1041 Baseline-normalized PP-EPSP amplitude. *Inset*, Representative traces for PP-EPSPs at the time indicated
1042 by arrowhead (black, 5 min; red, 45 min). **Bb**. Mean values for PP-EPSP amplitude. GSH in patch pipette
1043 solution did not change the PP-EPSP amplitude over time (0.66 ± 0.06 mV to 0.57 ± 0.11 mV, n = 5, t =
1044 0.040, p = 0.970, paired t-test). Comparison of these G_{in} and PP-EPSP amplitudes with those measured
1045 without GSH (reproduced from ref. 3) revealed that neither the baseline G_{in} nor PP-EPSPs was altered by
1046 intracellular GSH (G_{in} with GSH, 4.63 ± 1.47 nS, n = 14; G_{in} without GSH, 3.75 ± 0.51 nS, n = 9; t = -1.722, p
1047 = 0.100, independent t-test; PP-EPSP with GSH, 0.56 ± 0.04 mV, n = 7; PP-EPSP without GSH, 0.66 ± 0.05
1048 nS, n = 9; t = 1.512, p = 0.162 independent t-test). **Ca.** Representative membrane voltage responses to
1049 somatic ramp current injection (250 pA/s, black, at 5 min; red, at 45 min). **Cb.** The 1st AP latency remained

1050 stable (687.4 ± 78.73 ms to 662.4 ± 99.6 nS, n = 5, t = 0.362, p = 0.736, paired t-test). **Cc.** The AP threshold
1051 of CA3-PCs did not change throughout the recording in the presence of GSH. (-43.67 mV to -42.28 mV, n
1052 = 5, t = -1.16, p = 0.311, paired t-test).

1053

1054 *Fig. S3*

1055 **Fig. S3**, **The somatic or MF conditioning lowers the threshold for homosynaptic induction of LTP of PP-**
1056 **EPSCs (PP-LTP) in CA3-PCs**. WCRs of CA3-PCs were done using GSH-free patch pipette solution. **Aa** and **Ba**.
1057 Baseline-normalized amplitudes of PP-EPSPs (evoked every 10 s) were monitored before and after high-
1058 frequency stimulation of PP-CA3 synapses (PP-HFS, red arrow) with weak (*Aa*) or strong (*Ba*) stimulation
1059 intensity. PP-HFS is comprised of 10 bursts every 10 s, and each burst of 20 stimuli at 100 Hz. The
1060 stimulation intensity was quantified by the baseline PP-EPSC amplitude (weak, < 12.55 pA; strong, > 12.55
1061 pA). Upper red traces show voltage responses to PP-HFS. A single burst response was annotated as a gray
1062 box, and shown in the expanded time scale on the right. Note that weak PP-HFS induced neither APs (*Aa*)
1063 nor PP-LTP, whereas somatic APs were evoked during strong PP-HFS (*Ba*). EPSP amplitudes of non-failure
1064 events were normalized to the baseline value in the same cell. Recording times for the representative
1065 EPSC and EPSP traces (insets) are denoted in the main graph by the numbers (black, control; red, 30 min
1066 after PP-HFS). **Ab** and **Bb**. Mean amplitudes of PP-EPSC and PP-EPSP before and 30 min after PP-HFS in
1067 cases of PP-LTP induction failure (*Ab*), and in cases when LTP was induced (*Bb*). **C**. Plot of potentiation
1068 ratio of PP-EPSCs induced by PP-HFS as a function of the baseline EPSC amplitude, which is a metric of PP
1069 stimulation intensity. PP-LTP was induced in naïve CA3-PCs (gray symbols), and in CA3PCs that underwent
1070 MF (red) or somatic (blue) conditioning delivered before PP-HFS. A logistic function (baseline: 108.14 ±
1071 16.8%, max: 201.75 ± 29.6%, slope: 0.35578 ± 0.734, $EPSC_{50}$ = 13.077 ± 0.635 pA) was fitted to the LTP
1072 level of naïve CA3-PCs. **Da**. Voltage responses to weak PP-HFS in the CA3-PCs which underwent MF (upper,
1073 red) or somatic conditioning (lower, blue). The response to a single burst stimulation annotated as gray
1074 box is shown in the expanded time, in the right of each voltage responses. **Db**. PP-EPSC amplitude changes
1075 caused by MF or somatic conditioning (blue arrowhead) and subsequent PP-HFS (indicated by gray arrow
1076 at 0 min). Note that PP-LTP is readily induced by weak PP-HFS once the CA3-PC underwent MF (red
1077 symbols) or somatic (blue symbols) conditioning. **Dc**. Representative traces of PP-EPSCs (left) and PP-
1078 EPSPs (right) recorded at the times as indicated by the numbers in *Db* (black, baseline; blue, after MF
1079 (upper) or somatic (lower) conditioning; red, after PP-HFS). Note that MF or somatic conditioning

1080 enhanced PP-EPSPs but not PP-EPSCs, while both were enhanced by PP-HFS. **Ea-Eb**. Mean amplitudes of
1081 PP-EPSCs measured at the baseline, after MF (*Ea*) or somatic (*Eb*) conditioning, and after PP-HFS
1082 (conditioning: $F_{(1,19)} = 0.065$, $p = 0.802$, time: $F_{(1,19)} = 74.965$, $p < 0.001$, time × conditioning: $F_{(1,19)} = 0.012$,
1083 $p = 0.915$; GLM and simple effect analysis). **Ec-d**. Mean amplitudes of PP-EPSPs measured at the baseline,
1084 after MF (*Ec*) or somatic conditioning (*Ed*), and after PP-HFS (conditioning: $F_{(1,19)} = 3.856$, $p = 0.064$, time:
1085 $F_{(1,19)} = 11.858$, $p < 0.001$, time × conditioning: $F_{(1,19)} = 0.886$, $p = 0.358$; GLM and simple effect analysis).

1086

1087 *Fig. S4*

1088 **Fig. S4 Analysis of Fluorescence intensity of shEGFP(+) CA3-PCs. A**. Schematic timeline of the
1089 experimental procedure. *Upper*: Mice visited context A for 5 min and then returned to homecage for 85
1090 min, and sacrificed for *ex vivo* study (denoted as ctxA). *Lower*: After visiting context A for 5 min and being
1091 kept in homecage for 25 min, mice visited context B or C for 5 min, and then were kept in homecage for
1092 55 min before ex vivo study (denoted as ctxAB). **B**. Maximum intensity projection of Z-stack confocal
1093 images (Z_{max} image) of hippocampal CA3 region obtained from ctxA mice (Ba) and ctxAB mice (Bc). The
1094 right graph of each image shows the fluorescence intensity profiles of boxed GFP(+) CA3-PCs as a function
1095 of depth from a surface the slices. The same color codes are used for each box and corresponding profile.
1096 Fluorescence signals above a threshold of 5× the SD of baseline fluctuation were regarded as a
1097 fluorescence signal of GFP(+) CA3-PCs. **C**. Plot of maximum fluorescence intensity (F_{max}) of individual
1098 GFP(+) CA3-PCs as a function of the depth at which F_{max} of each cell was measured. Distribution of GFP
1099 fluorescence measured in GFP(+) CA3-PCs from ctxAB or ctxAC mice was bimodal, in contrast to those of
1100 ctxA mice, and thus CA3-PCs from ctxAB or ctxAC mice were clustered into two groups: cells displaying
1101 low or high GFP fluorescence. **Cb**. Mean fluorescence of GFP(+) CA3-PCs measured in different cell groups.
1102 There was no significant difference in the fluorescence intensity between high fluorescence ctx AB and
1103 ctx AC cells. **D.** Histogram of fluorescence intensity of shEGFP(+) CA3-PCs from either ctxA (*Da*) or ctxAB
1104 (*Db*) mice. In each plot, mono- and bi-lognormal fits are shown. Mono- and bi-lognormal fits were better
1105 for ctxA and ctxAB, respectively. The best fit parameters of log-normal function [$y = A*\exp[-(\ln(x/m)/s)^2]$]
1106 for ctxA: $A = 11.6$, $m = 37.6$, $s = 1.24$. Those for ctxAB, $A_1 = 7.41$, $m_1 = 55.87$, $s_1 = 1.106$, $A_2 = 1.497$, $m_2 =$
1107 521.6, s2 = 0.29.

Fig. S5.

Fig. S5, A. Connectivity map between PCs and INs (blue, not connected; light blue, connected). PCs are indexed from 1 to 1000, and INs are from 1001 to 1200. The baseline synaptic conductance between PCs (J_{ee}) was set to a random value between 0 and 0.35 nS. The synaptic conductance values for PCs-to-INs (J_{ie}), INs-to-PCs (J_{ei}), INs-to-INs (J_{ii}) were set to 0.4 nS. c, connection probability; J, baseline synaptic weight; e, excitatory; i, inhibitory; J_{YX}, synaptic conductance from X to Y. **Ba-Bb**, STDP rule at A/C and PP synapses. The LTP ratio (L), was modelled as, $L(\Delta t) = 2 \exp(-|\Delta t|/40)$ for A/C synapses. For PP synapses, $L(\Delta t) = 2 \exp(-\Delta t/30)$ if $\Delta t \geq 0$, and $-0.5 \exp(\Delta t/15)$ if $\Delta t < 0$. **C**, To emulate a distal dendritic spike elicited by PP inputs to a primed PC (Hyun et al., 2015), the inward current pulse was injected upon arrival of PP inputs in a primed PC (Jahnke et al., 2015). **D**, Distributions of the number of MF and PP inputs to each CA3-PC per a pattern. Left, the number of MF inputs to a CA3-PC in an active **M** subset was set to a random number which follows log-normal distribution with $\mu = 1$ and $\sigma = 0.6$. The MF input numbers were bounded by [3, 15]. Right, Distributions for the number of PP inputs during recall and encoding phases are compared (red and blue bars, respectively). The PP input numbers were also set by random values of lognormal distribution with $\mu = 1.8$ and $\sigma = 0.3$ for encoding phase [number of inputs, 6.33 ± 3.77 (mean $\pm$ variance)], and by those with $\mu = 1.2$ and $\sigma = 0.3$ for recall phase [number of inputs, 3.47 ± 1.14]. The number of PP inputs was bounded by [3, 20] for encoding, and by [0, 10] for recall. **E**, The cue input incoming via PP that triggers retrieval of $\mathbf{M_1}$. The PP inputs are light-blue colored if the synaptic weights have been strengthened during the encoding phase, and magenta otherwise.

1128 ## References

1129 Bennett, M. R., Gibson, W. G., & Robinson, J. (1994). Dynamics of the CA3 pyramidal neuron
1130 autoassociative memory network in the hippocampus *Philos Trans R Soc Lond B Biol Sci*, *29*, 11.
1131 Blanchetot, C., Tertoolen, L. G., & den Hertog, J. (2002). Regulation of receptor protein-tyrosine
1132 phosphatase alpha by oxidative stress. . *The EMBO journal*, *21*(4), 11.
1133 https://doi.org/https://doi.org/10.1093/emboj/21.4.493
1134 Brandt, D., Goerke, A., Heuer, M., Gimona, M., Leitges, M., Kremmer, E., . . . Mischak, H. (2003). Protein
1135 kinase C delta induces Src kinase activity via activation of the protein tyrosine phosphatase PTP
1136 alpha. *J Biol Chem*, *278*(36), 34073-34078. https://doi.org/10.1074/jbc.M211650200
1137 Buzsaki, G., & Mizuseki, K. (2014). The log-dynamic brain: how skewed distributions affect network
1138 operations. *Nat Rev Neurosci*, *15*(4), 264-278. https://doi.org/10.1038/nrn3687
1139 Cai, D. J., Aharoni, D., Shuman, T., Shobe, J., Biane, J., Song, W., . . . Silva, A. J. (2016). A shared neural
1140 ensemble links distinct contextual memories encoded close in time. *Nature*, *534*(7605), 115-118.
1141 https://doi.org/10.1038/nature17955
1142 Chen, X., Yuan, L. L., Zhao, C., Birnbaum, S. G., Frick, A., Jung, W. E., . . . Johnston, D. (2006). Deletion of
1143 Kv4.2 gene eliminates dendritic A-type K+ current and enhances induction of long-term
1144 potentiation in hippocampal CA1 pyramidal neurons. *J Neurosci*, *26*(47), 12143-12151.
1145 https://doi.org/10.1523/JNEUROSCI.2667-06.2006
1146 Dong, Y., Green, T., Saal, D., Marie, H., Neve, R., Nestler, E. J., & Malenka, R. C. (2006). CREB modulates
1147 excitability of nucleus accumbens neurons. *Nat Neurosci*, *9*(4), 475-477.
1148 https://doi.org/10.1038/nn1661
1149 Eom, K., Hyun, J. H., Lee, D. G., Kim, S., Jeong, H. J., Kang, J. S., . . . Lee, S. H. (2019). Intracellular Zn(2+)
1150 Signaling Facilitates Mossy Fiber Input-Induced Heterosynaptic Potentiation of Direct Cortical
1151 Inputs in Hippocampal CA3 Pyramidal Cells. *J Neurosci*, *39*(20), 3812-3831.
1152 https://doi.org/10.1523/JNEUROSCI.2130-18.2019
1153 Eom, K., Lee, H. R., Hyun, J. H., An, H., Lee, Y. S., Ho, W. K., & Lee, S. H. (2022). Gradual decorrelation of
1154 CA3 ensembles associated with contextual discrimination learning is impaired by Kv1.2
1155 insufficiency. *Hippocampus*, *32*(3), 193-216. https://doi.org/10.1002/hipo.23400
1156 Farovik, A., Dupont, L. M., & Eichenbaum, H. (2010). Distinct roles for dorsal CA3 and CA1 in memory for
1157 sequential nonspatial events. *Learn Mem*, *17*(1), 12-17. https://doi.org/10.1101/lm.1616209
1158 Forman, H. J., Zhang, H., & Rinna, A. (2009). Glutathione: overview of its protective roles, measurement,
1159 and biosynthesis. *Mol Aspects Med*, *30*(1-2), 1-12. https://doi.org/10.1016/j.mam.2008.08.006
1160 Garcia, A. J., 3rd, Putnam, R. W., & Dean, J. B. (2010). Hyperoxic stimulation of synchronous orthodromic
1161 activity and induction of neural plasticity does not require changes in excitatory synaptic
1162 transmission. *J Appl Physiol (1985)*, *109*(3), 820-829.
1163 https://doi.org/10.1152/japplphysiol.91430.2008
1164 Grishin, A. A., Benquet, P., & Gerber, U. (2005). Muscarinic receptor stimulation reduces NMDA responses
1165 in CA3 hippocampal pyramidal cells via Ca2+-dependent activation of tyrosine phosphatase.
1166 *Neuropharmacology*, *49*(3), 328-337. https://doi.org/10.1016/j.neuropharm.2005.03.019
1167 Guzman, S., Schlögl, A., Frotscher, M., & Jonas, P. (2016). Synaptic mechanisms of pattern completion in
1168 the hippocampal CA3 network. *Science*, *353*, 1117-1123.
1169 Hasselmo, M. E. (2006). The role of acetylcholine in learning and memory. *Curr Opin Neurobiol*, *16*(6), 710-
1170 715. https://doi.org/10.1016/j.conb.2006.09.002
1171 Henze, D., Wittner, L., & Buzsaki, G. (2002). Single granule cells reliably discharge targets in the
1172 hippocampal CA3 network in vivo. *Nat Neurosci*, *5*(8), 790-795. https://doi.org/10.1038/nn887

Hunsaker, M. R., & Kesner, R. P. (2013). The operation of pattern separation and pattern completion processes associated with different attributes or domains of memory. *Neurosci Biobehav Rev*, *37*(1), 36-58. https://doi.org/10.1016/j.neubiorev.2012.09.014

Hurvich, C. M., & Tsai, C. L. (1989). Regression and Time-Series Model Selection in Small Samples. *Biometrika*, *76*(2), 297-307. https://doi.org/DOI 10.1093/biomet/76.2.297

Hyun, J., Eom, K., Lee, K., Bae, J., Bae, Y., Kim, M., . . . Lee, S. (2015). Kv1.2 mediates heterosynaptic modulation of direct cortical synaptic inputs in CA3 pyramidal cells. *J Physiol*, *593*(16), 3617-3643. https://doi.org/10.1113/JP270372

Hyun, J., Eom, K., Lee, K., Ho, W., & Lee, S. (2013). Activity-dependent downregulation of D-type K+ channel subunit Kv1.2 in rat hippocampal CA3 pyramidal neurons. *J Physiol*, *591*(22), 5525-5540. https://doi.org/10.1113/jphysiol.2013.259002

Ikegaya, Y., Sasaki, T., Ishikawa, D., Honma, N., Tao, K., Takahashi, N., . . . Matsuki, N. (2013). Interpyramid spike transmission stabilizes the sparseness of recurrent network activity. *Cereb Cortex*, *23*(2), 293-304. https://doi.org/10.1093/cercor/bhs006

Jahnke, S., Timme, M., & Memmesheimer, R. M. (2015). A Unified Dynamic Model for Learning, Replay, and Sharp-Wave/Ripples. *J Neurosci*, *35*(49), 16236-16258. https://doi.org/10.1523/JNEUROSCI.3977-14.2015

Jonas, P., Major, G., & Sakmann, B. (1993). Quantal components of unitary EPSCs at the mossy fibre synapse on CA3 pyramidal cells of rat hippocampus. *J Physiol.*, *472*, 49.

Kastellakis, G., Silva, A. J., & Poirazi, P. (2016). Linking Memories across Time via Neuronal and Dendritic Overlaps in Model Neurons with Active Dendrites. *Cell Rep*, *17*(6), 1491-1504. https://doi.org/10.1016/j.celrep.2016.10.015

Kohus, Z., Kali, S., Rovira-Esteban, L., Schlingloff, D., Papp, O., Freund, T. F., . . . Gulyas, A. I. (2016). Properties and dynamics of inhibitory synaptic communication within the CA3 microcircuits of pyramidal cells and interneurons expressing parvalbumin or cholecystokinin. *J Physiol*, *594*(13), 3745-3774. https://doi.org/10.1113/JP272231

Kowalski, J., Gan, J., Jonas, P., & Pernia-Andrade, A. J. (2016). Intrinsic membrane properties determine hippocampal differential firing pattern in vivo in anesthetized rats. *Hippocampus*, *26*(5), 668-682. https://doi.org/10.1002/hipo.22550

Lee, D., Hyun, J. H., Jung, K., Hannan, P., & Kwon, H. B. (2017). A calcium- and light-gated switch to induce gene expression in activated neurons. *Nat Biotechnol*, *35*(9), 858-863. https://doi.org/10.1038/nbt.3902

Lee, I., & Kesner, R. P. (2004). Encoding versus retrieval of spatial memory: Double dissociation between the dentate gyrus and the perforant path inputs into CA3 in the dorsal hippocampus. *Hippocampus*, *14*(1), 66-76. https://doi.org/DOI 10.1002/hipo.10167

Lev, S., Moreno, H., Martinez , R., Canoll, P., Peles, E., Musacchio, J., . . . Schlessinger, J. (1995). Protein tyrosine kinase PYK2 involved in Ca2+-induced regulation of ion channel and MAP kinase functions. *Nature*, *376*, 737-745.

Levy, W. B., Hocking, A. B., & Wu, X. (2005). Interpreting hippocampal function as recoding and forecasting. *Neural Networks*, *18*, 23.

Lisman, J., Cooper, K., Sehgal, M., & Silva, A. J. (2018). Memory formation depends on both synapse-specific modifications of synaptic strength and cell-specific increases in excitability. *Nat Neurosci*, *21*(3), 309-314. https://doi.org/10.1038/s41593-018-0076-6

Lopez de Armentia, M., Jancic, D., Olivares, R., Alarcon, J. M., Kandel, E. R., & Barco, A. (2007). cAMP response element-binding protein-mediated gene expression increases the intrinsic excitability of CA1 pyramidal neurons. *J Neurosci*, *27*(50), 13909-13918. https://doi.org/10.1523/JNEUROSCI.3850-07.2007

Malezieux, M., Kees, A. L., & Mulle, C. (2020). Theta Oscillations Coincide with Sustained Hyperpolarization in CA3 Pyramidal Cells, Underlying Decreased Firing. *Cell Rep*, *32*(1), 107868. https://doi.org/10.1016/j.celrep.2020.107868

McMahon, D., & Barrionuevo, G. (2002). Short- and long-term plasticity of the perforant path synapse in hippocampal area CA3. *J Neurophysiol*, *88*, 528-533.

McNaughton, B. L., & Morris, R. G. (1987). Hippocampal synaptic enhancement and information storage within a distributed memory system. *Trends in neurosciences*, *10*(10), 8.

Meng, T., Fukada, T., & Tonks, N. (2002). Reversible oxidation and inactivation of protein tyrosine phosphatases in vivo. . *Mol Cell*, *9*(2), 13. https://doi.org/https://doi.org/10.1016/s1097-2765(02)00445-8

Mishra, R. K., Kim, S., Guzman, S. J., & Jonas, P. (2016). Symmetric spike timing-dependent plasticity at CA3-CA3 synapses optimizes storage and recall in autoassociative networks. *Nat Commun*, *7*, 11552. https://doi.org/10.1038/ncomms11552

Moeyaert, B., Holt, G., Madangopal, R., Perez-Alvarez, A., Fearey, B. C., Trojanowski, N. F., . . . Schreiter, E. R. (2018). Improved methods for marking active neuron populations. *Nat Commun*, *9*(1), 4440. https://doi.org/10.1038/s41467-018-06935-2

Moser, E. I., Krobert, K. A., Moser, M. B., & Morris, R. G. (1998). Impaired spatial learning after saturation of long-term potentiation. *Science*, *281*(5385), 2038-2042. https://doi.org/10.1126/science.281.5385.2038

O'Reilly, R. C., & McClelland, J. L. (1994). Hippocampal conjunctive encoding, storage, and recall: avoiding a trade-off. *Hippocampus*, *4*, 661-682.

Oh, M. M., & Disterhoft, J. F. (2015). Increased Excitability of Both Principal Neurons and Interneurons during Associative Learning. *Neuroscientist*, *21*(4), 372-384. https://doi.org/10.1177/1073858414537382

Perez-Rosello, T., Baker, J., Ferrante, M., Iyengar, S., Ascoli, G., & Barrionuevo, G. (2011). Passive and active shaping of unitary responses from associational/commissural and perforant path synapses in hippocampal CA3 pyramidal cells. . *J Comp Neurosci 31,* , 159-182. https://doi.org/10.1007/s10827-010-0303-y)

Pignatelli, M., Ryan, T. J., Roy, D. S., Lovett, C., Smith, L. M., Muralidhar, S., & Tonegawa, S. (2019). Engram Cell Excitability State Determines the Efficacy of Memory Retrieval. *Neuron*, *101*(2), 274-284 e275. https://doi.org/10.1016/j.neuron.2018.11.029

Rashid, A. J., Yan, C., Mercaldo, V., Hsiang, H. L., Park, S., Cole, C. J., . . . Josselyn, S. A. (2016). Competition between engrams influences fear memory formation and recall. *Science*, *353*(6297), 383-387. https://doi.org/10.1126/science.aaf0594

Shigemoto, R., Kinoshita, A., Wada, E., Nomura, S., Ohishi, H., Takada, M., . . . Mizuno, N. (1997). Differential Presynaptic Localization of Metabotropic Glutamate Receptor Subtypes in the Rat Hippocampus. *The Journal of neuroscience*, *17*(19), 20.

Silva, A. J., Zhou, Y., Rogerson, T., Shobe, J., & Balaji, J. (2009). Molecular and cellular approaches to memory allocation in neural circuits. *Science*, *326*(5951), 391-395. https://doi.org/10.1126/science.1174519

Sorensen, A. T., Cooper, Y. A., Baratta, M. V., Weng, F. J., Zhang, Y., Ramamoorthi, K., . . . Lin, Y. (2016). A robust activity marking system for exploring active neuronal ensembles. *Elife*, *5*. https://doi.org/10.7554/eLife.13918

Treves, A., & Rolls, E. (1992). Computational constraints suggest the need for two distinct input systems to the hippocampal CA3 network. . *Hippocampus*, *2*, 189-199.

1265 Tsai, W., Morielli, A., Cachero, T., & Peralta, E. (1998). Receptor protein tyrosine phosphatase alpha
1266 participates in the m1 muscarinic acetylcholine receptor-dependent regulation of Kv1.2 channel
1267 activity. *EMBO*, *18,*, 109-118.
1268 Tsukamoto, M., Yasui, T., Yamada, M. K., Nishiyama, N., Matsuki, N., & Ikegaya, Y. (2003). Mossy fibre
1269 synaptic NMDA receptors trigger non-hebbian long-term potentiation at entorhino-CA3 synapses
1270 in the rat. *The Journal of Physiology*, *546*(3), 665-675.
1271 https://doi.org/10.1113/jphysiol.2002.033803
1272 Vogt, K., & Regehr, W. (2001). Cholinergic modulation of excitatory synaptic transmission in the CA3 area
1273 of the hippocampus. *The Journal of neuroscience*, *21*(1), 9.
1274 https://doi.org/https://doi.org/10.1523/JNEUROSCI.21-01-00075.2001
1275 Wallenstein, G. V., Eichenbaum, H., & Hasselmo, M. E. (1998). The hippocampus as an associator of
1276 discontiguous events *Trends Neurosci*, *21*, 7.
1277 Yoon, J. Y., Lee, H. R., Ho, W. K., & Lee, S. H. (2020). Disparities in Short-Term Depression Among Prefrontal
1278 Cortex Synapses Sustain Persistent Activity in a Balanced Network. *Cereb Cortex*, *30*(1), 113-134.
1279 https://doi.org/10.1093/cercor/bhz076

1280

Fig. 1

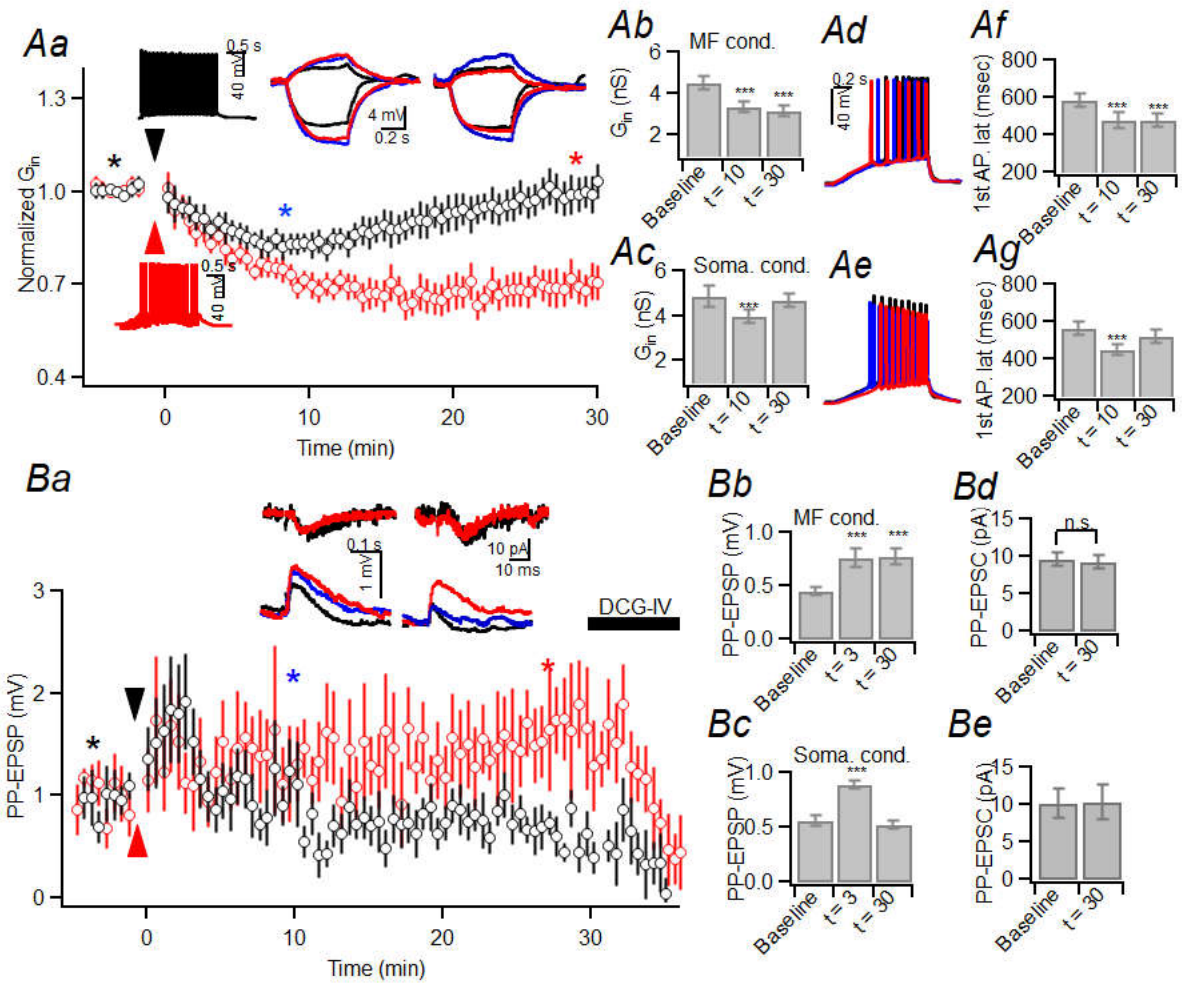
Aa
Normalized G_{in}
Time (min)
0.5 s
40 mV
4 mV
0.2 s
Ab
MF cond.
G_{in} (nS)
Baseline
t = 10
t = 30
Ac
Soma. cond.
Ad
Ae
Af
1st AP. lat (msec)
Ag
Ba
PP-EPSP (mV)
0.1 s
1 mV
10 pA
10 ms
DCG-IV
Bb
MF cond.
t = 3
Bc
Soma. cond.
Bd
PP-EPSC (pA)
n.s.
Be

Fig. 2

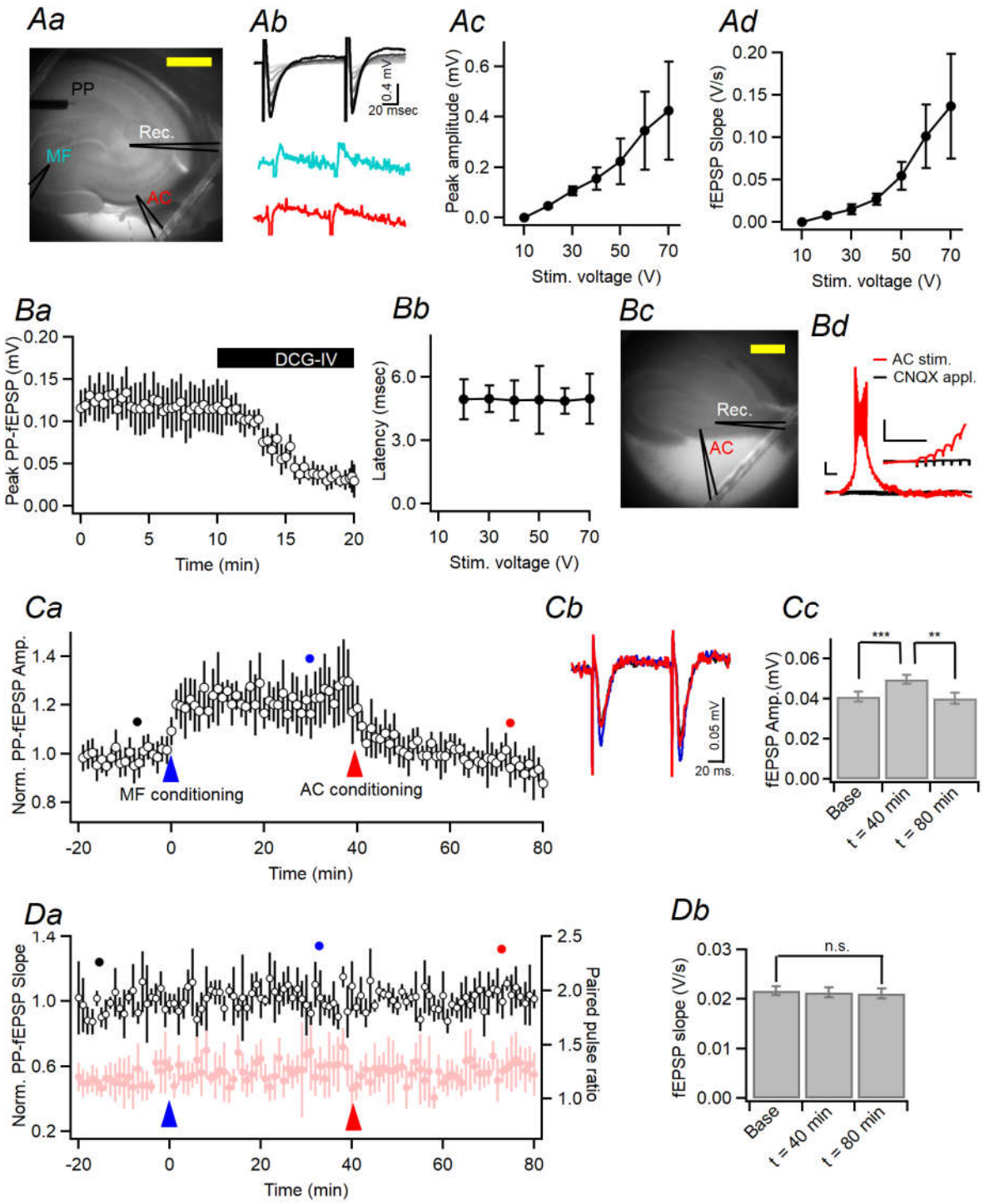
Aa
PP
Rec.
MF
AC
Ab
0.4 mV
20 msec
Ac
Peak amplitude (mV)
Stim. voltage (V)
Ad
fEPSP Slope (V/s)
Stim. voltage (V)
Ba
DCG-IV
Peak PP-fEPSP (mV)
Time (min)
Bb
Latency (msec)
Stim. voltage (V)
Bc
Rec.
AC
Bd
AC stim.
CNQX appl.
Ca
Norm. PP-fEPSP Amp.
MF conditioning
AC conditioning
Time (min)
Cb
0.05 mV
20 ms.
Cc
fEPSP Amp.(mV)
Base
t = 40 min
t = 80 min
Da
Norm. PP-fEPSP Slope
Paired pulse ratio
Time (min)
Db
fEPSP slope (V/s)
n.s.
Base
t = 40 min
t = 80 min

Fig. 3

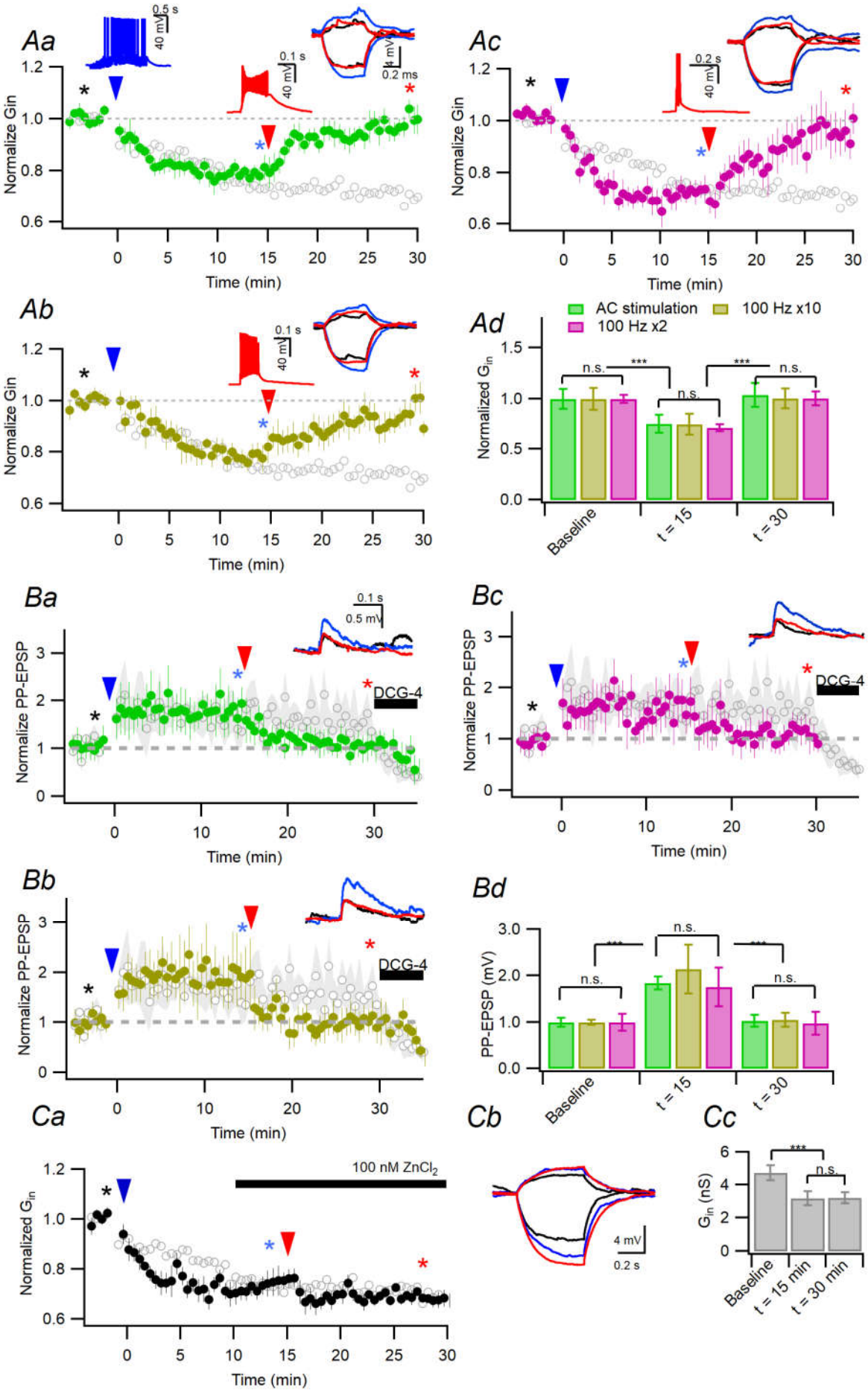
Aa
Ac
Ab
Ad
Ba
Bc
Bb
Bd
Ca
Cb
Cc
Normalize Gin
Time (min)
0.5 s
40 mV
0.1 s
0.2 ms
0.2 s
AC stimulation
100 Hz x10
100 Hz x2
Normalized Gin
n.s.
***
Baseline
t = 15
t = 30
Normalize PP-EPSP
DCG-4
0.5 mV
PP-EPSP (mV)
100 nM ZnCl2
4 mV
Gin (nS)
t = 15 min
t = 30 min

Fig. 4

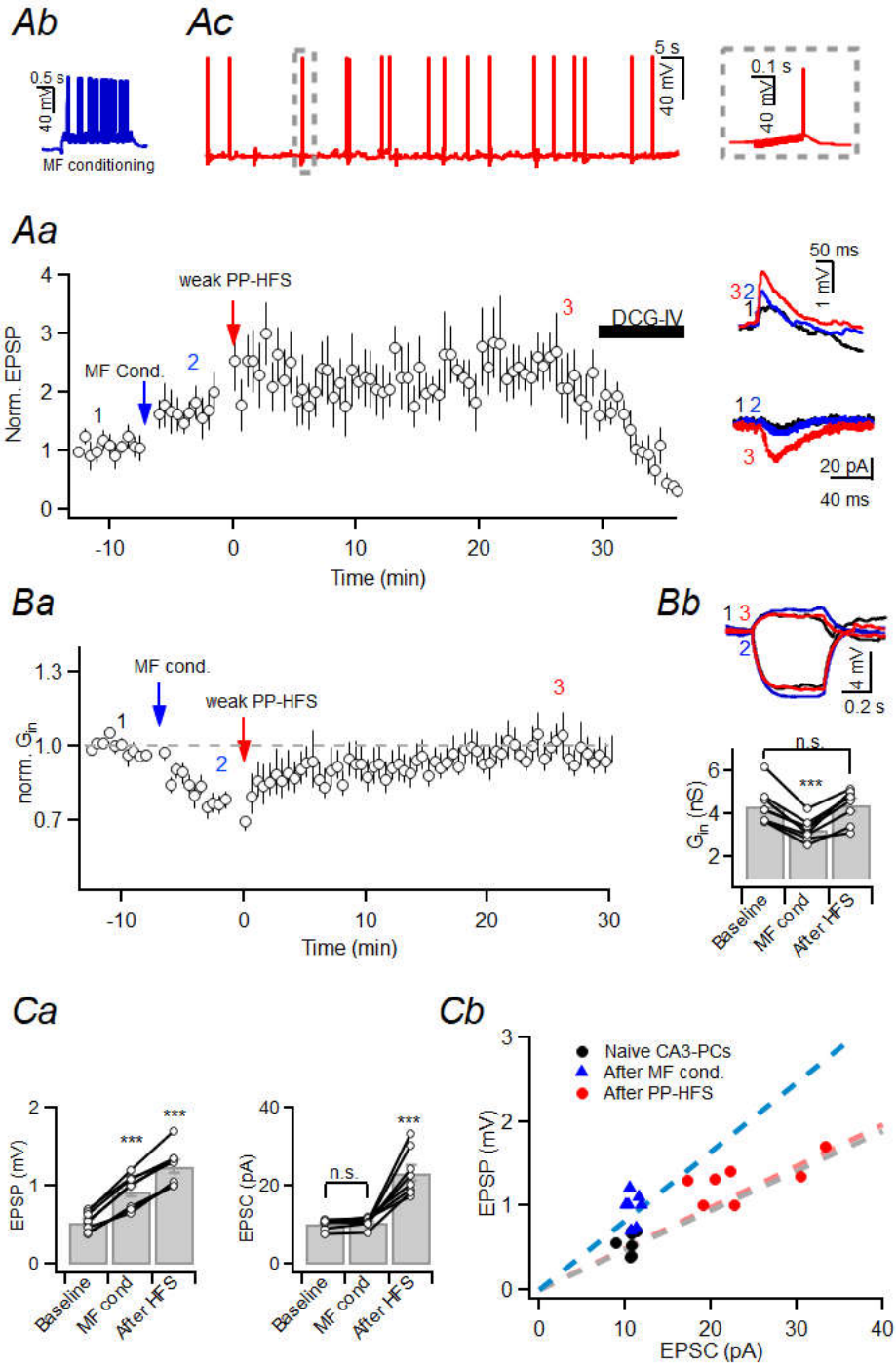
Ab
Ac
0.5 s
40 mV
MF conditioning
5 s
40 mV
0.1 s
40 mV
Aa
weak PP-HFS
MF Cond.
DCG-IV
Norm. EPSP
Time (min)
50 ms
1 mV
20 pA
40 ms
Ba
MF cond.
weak PP-HFS
norm. G_{in}
Time (min)
Bb
4 mV
0.2 s
n.s.
***
G_{in} (nS)
Baseline
MF cond
After HFS
Ca
EPSP (mV)
EPSC (pA)
n.s.
Cb
Naive CA3-PCs
After MF cond.
After PP-HFS
EPSP (mV)
EPSC (pA)

Fig. 5

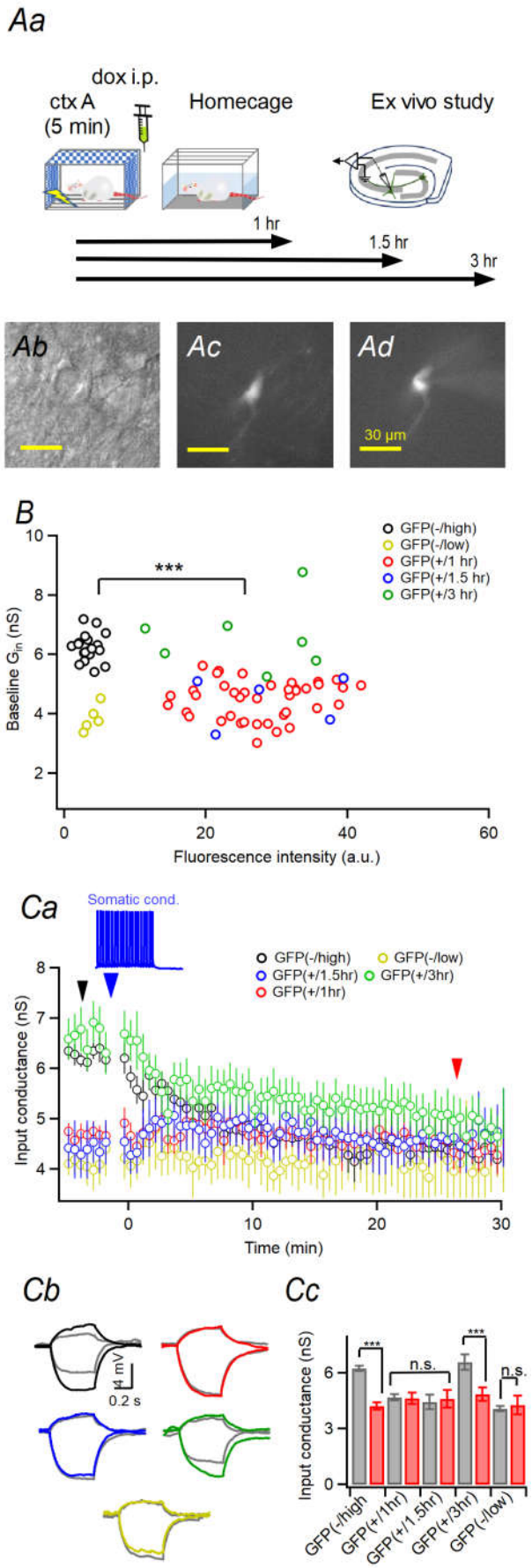
Aa
dox i.p.
ctx A
(5 min)
Homecage
Ex vivo study
1 hr
1.5 hr
3 hr
Ab
Ac
Ad
30 µm
B
GFP(-/high)
GFP(-/low)
GFP(+/1 hr)
GFP(+/1.5 hr)
GFP(+/3 hr)
***
Baseline G_{in} (nS)
Fluorescence intensity (a.u.)
Ca
Somatic cond.
GFP(-/high)
GFP(-/low)
GFP(+/1.5hr)
GFP(+/3hr)
GFP(+/1hr)
Input conductance (nS)
Time (min)
Cb
4 mV
0.2 s
Cc
***
n.s.
***
n.s.
Input conductance (nS)
GFP(-/high
GFP(+/1hr)
GFP(+/1.5hr)
GFP(+/3hr)
GFP(-/low)

Fig. 6

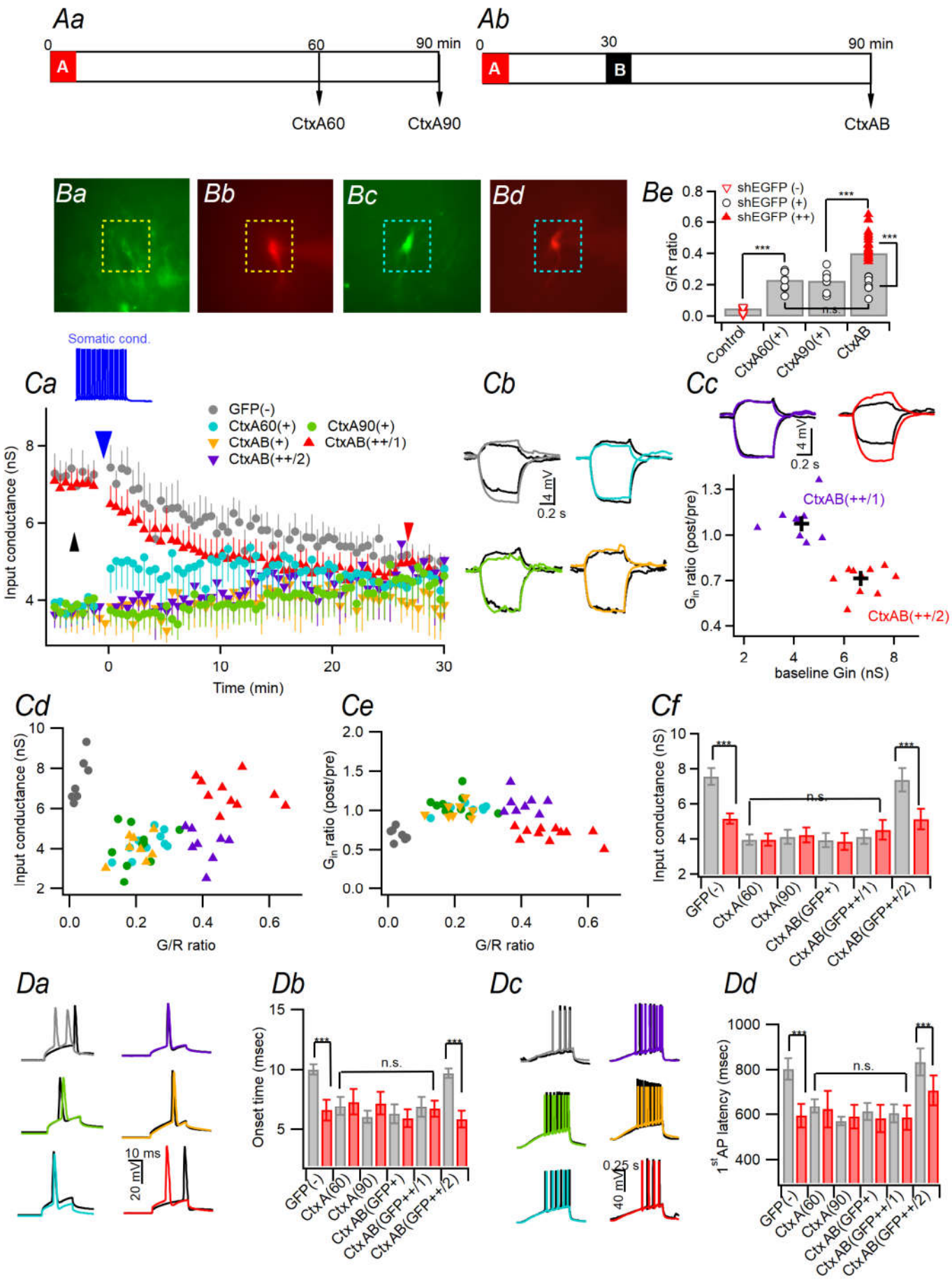
Aa
0
60
90 min
A
CtxA60
CtxA90
Ab
0
30
90 min
A
B
CtxAB
Ba
Bb
Bc
Bd
Be
shEGFP (-)
shEGFP (+)
shEGFP (++)
G/R ratio
Control
CtxA60(+)
CtxA90(+)
CtxAB
n.s.
Somatic cond.
Ca
GFP(-)
CtxA60(+)
CtxA90(+)
CtxAB(+)
CtxAB(++/1)
CtxAB(++/2)
Input conductance (nS)
Time (min)
Cb
4 mV
0.2 s
Cc
4 mV
0.2 s
CtxAB(++/1)
CtxAB(++/2)
Gin ratio (post/pre)
baseline Gin (nS)
Cd
Input conductance (nS)
G/R ratio
Ce
Gin ratio (post/pre)
G/R ratio
Cf
Input conductance (nS)
n.s.
GFP(-)
CtxA(60)
CtxA(90)
CtxAB(GFP+)
CtxAB(GFP++/1)
CtxAB(GFP++/2)
Da
10 ms
20 mV
Db
Onset time (msec)
n.s.
Dc
0.25 s
40 mV
Dd
1st AP latency (msec)
n.s.

Fig. 7

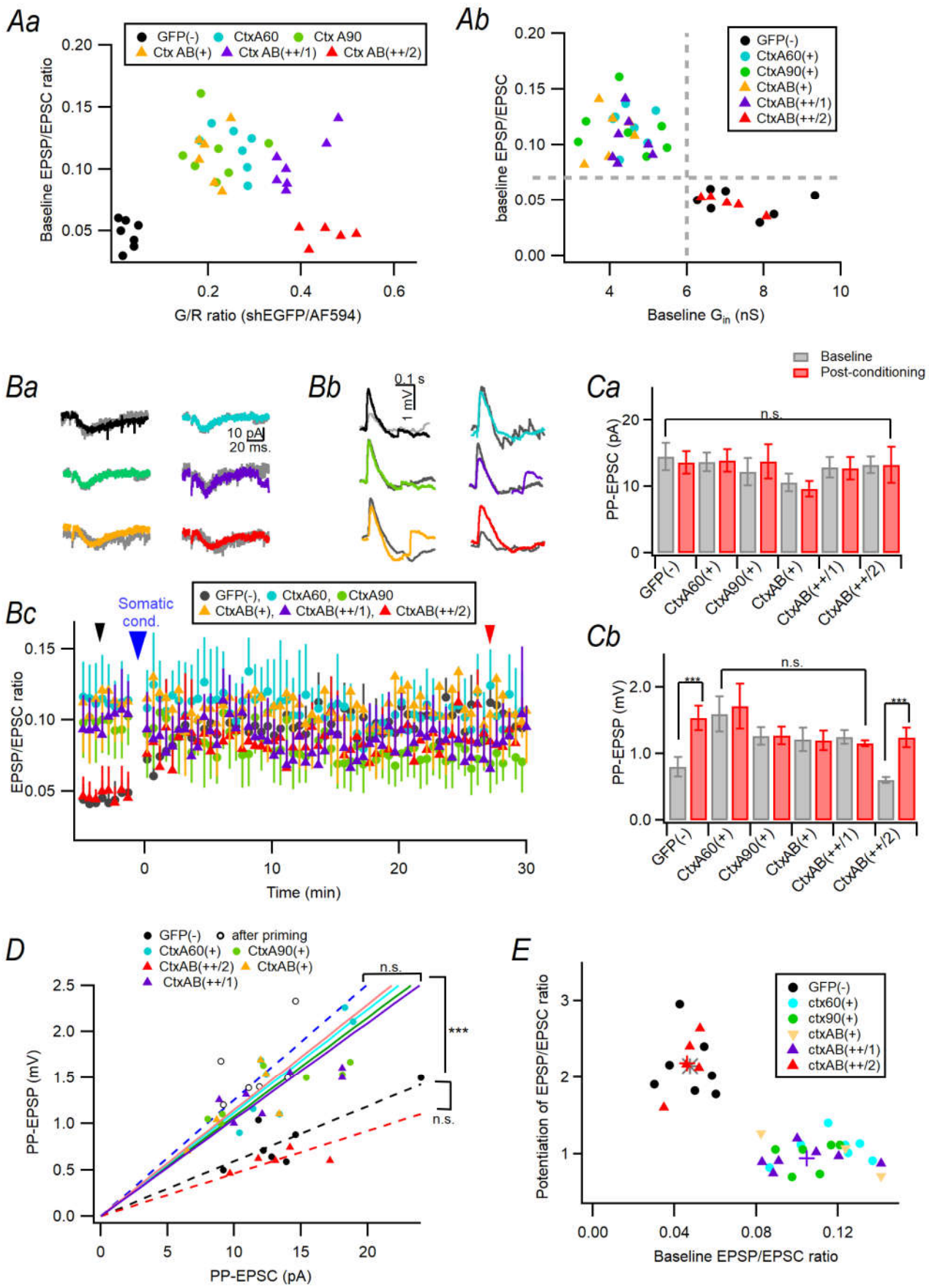
Aa
GFP(-)
CtxA60
Ctx A90
Ctx AB(+)
Ctx AB(++/1)
Ctx AB(++/2)
Baseline EPSP/EPSC ratio
G/R ratio (shEGFP/AF594)
Ab
GFP(-)
CtxA60(+)
CtxA90(+)
CtxAB(+)
CtxAB(++/1)
CtxAB(++/2)
baseline EPSP/EPSC
Baseline G_in (nS)
Ba
10 pA
20 ms
Bb
0.1 s
1 mV
Ca
Baseline
Post-conditioning
n.s.
PP-EPSC (pA)
GFP(-)
CtxA60(+)
CtxA90(+)
CtxAB(+)
CtxAB(++/1)
CtxAB(++/2)
Bc
Somatic cond.
GFP(-), CtxA60, CtxA90
CtxAB(+), CtxAB(++/1), CtxAB(++/2)
EPSP/EPSC ratio
Time (min)
Cb
n.s.
***
PP-EPSP (mV)
D
GFP(-)
after priming
CtxA60(+)
CtxA90(+)
CtxAB(++/2)
CtxAB(+)
CtxAB(++/1)
n.s.
***
PP-EPSP (mV)
PP-EPSC (pA)
E
GFP(-)
ctx60(+)
ctx90(+)
ctxAB(+)
ctxAB(++/1)
ctxAB(++/2)
Potentiation of EPSP/EPSC ratio
Baseline EPSP/EPSC ratio

Fig. 8

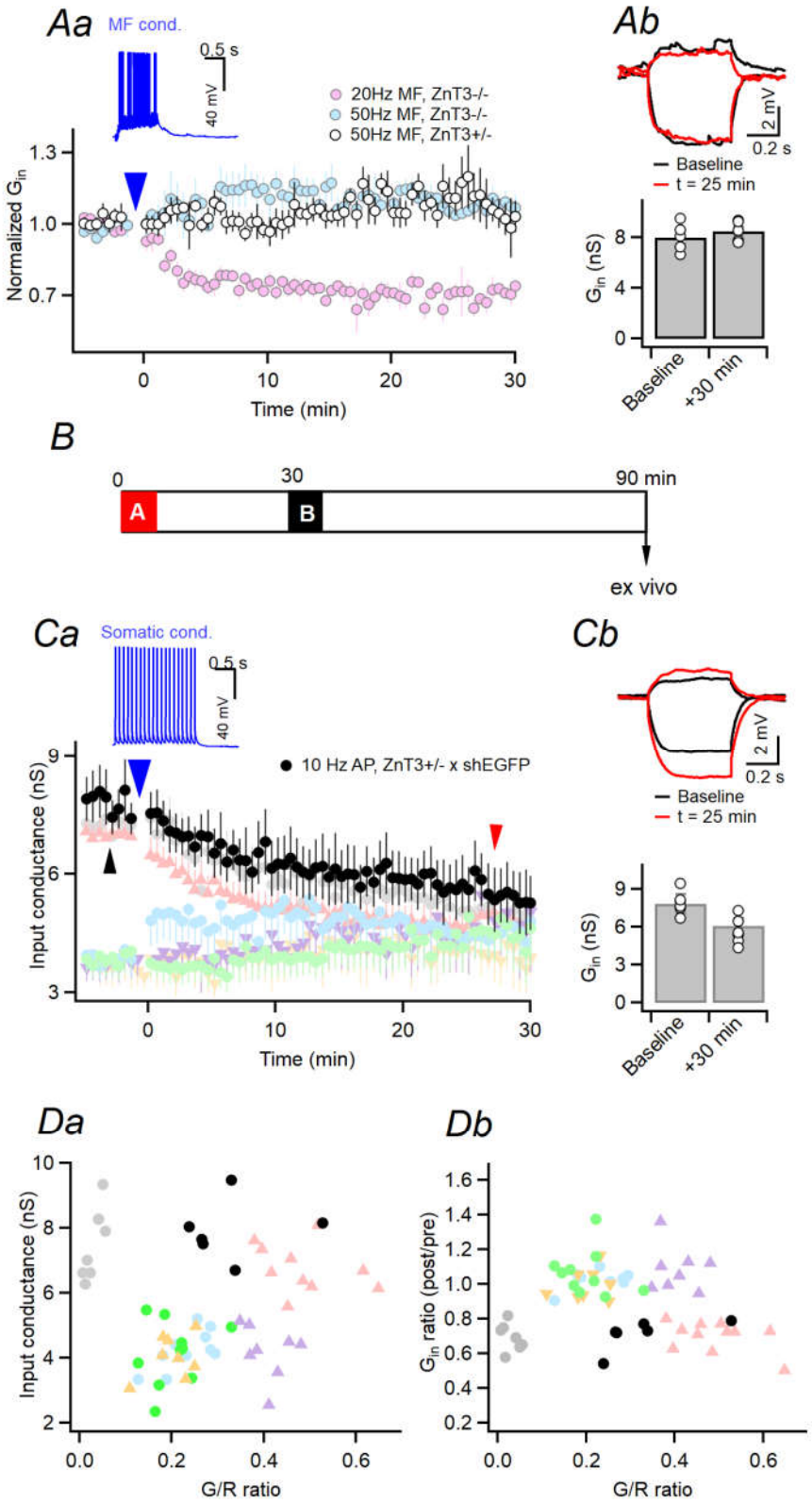
Aa
MF cond.
0.5 s
40 mV
20Hz MF, ZnT3-/-
50Hz MF, ZnT3-/-
50Hz MF, ZnT3+/-
Normalized G_{in}
1.3
1.0
0.7
0
10
20
30
Time (min)
Ab
2 mV
0.2 s
Baseline
t = 25 min
G_{in} (nS)
8
4
0
Baseline
+30 min
B
0
30
90 min
A
B
ex vivo
Ca
Somatic cond.
0.5 s
40 mV
10 Hz AP, ZnT3+/- x shEGFP
Input conductance (nS)
9
6
3
0
10
20
30
Time (min)
Cb
2 mV
0.2 s
Baseline
t = 25 min
G_{in} (nS)
9
6
3
0
Baseline
+30 min
Da
Input conductance (nS)
10
8
6
4
2
0.0
0.2
0.4
0.6
G/R ratio
Db
G_{in} ratio (post/pre)
1.6
1.4
1.2
1.0
0.8
0.6
0.4
0.2
0.0
0.2
0.4
0.6
G/R ratio

Fig. 9

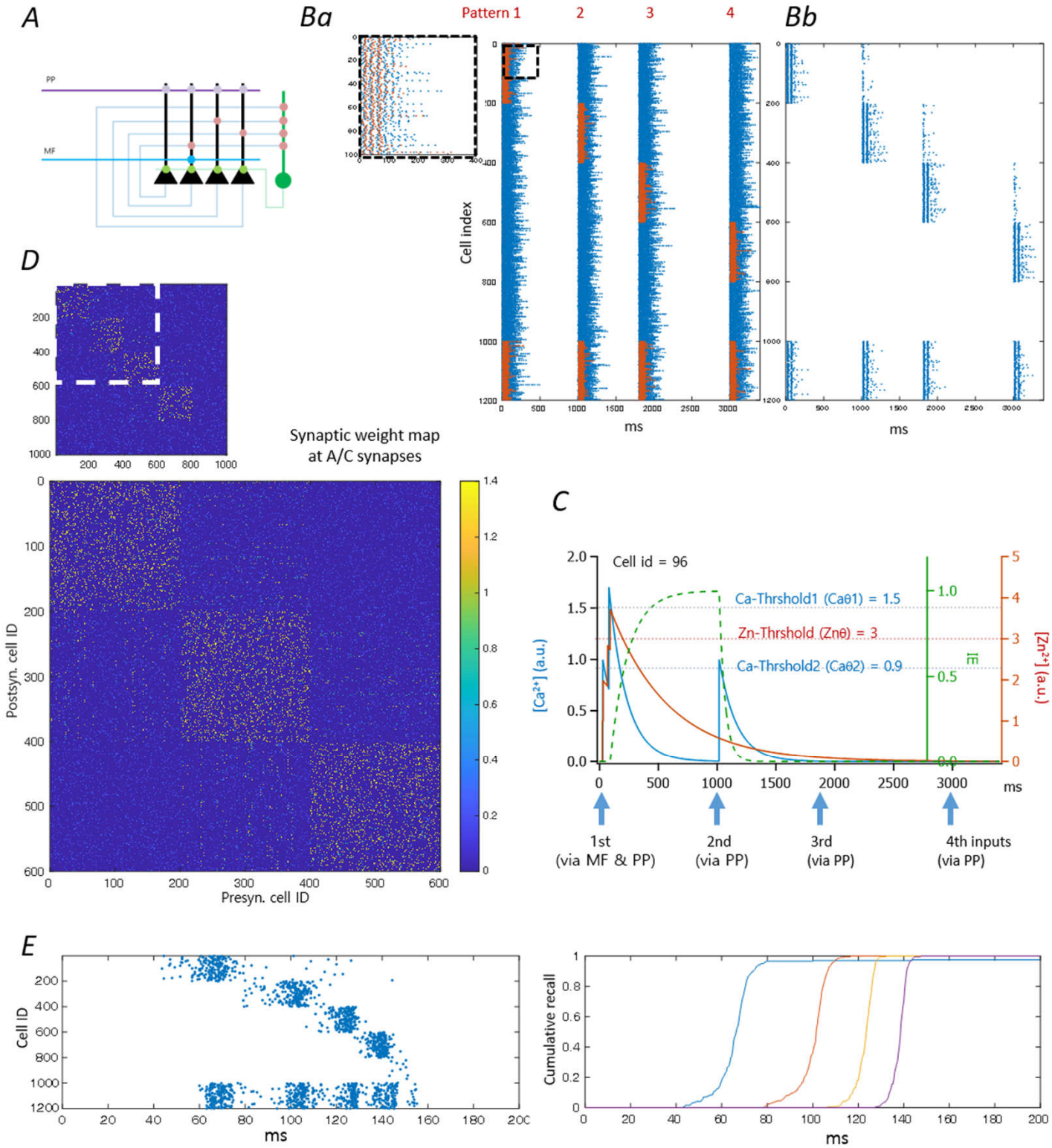
A
PP
MF
Ba
Pattern 1
2
3
4
Cell index
ms
Bb
ms
D
Synaptic weight map
at A/C synapses
Postsyn. cell ID
Presyn. cell ID
C
Cell id = 96
Ca-Thrshold1 (Caθ1) = 1.5
Zn-Thrshold (Znθ) = 3
Ca-Thrshold2 (Caθ2) = 0.9
[Ca2+] (a.u.)
[Zn2+] (a.u.)
ms
1st
(via MF & PP)
2nd
(via PP)
3rd
(via PP)
4th inputs
(via PP)
E
Cell ID
ms
Cumulative recall
ms

Fig. S1

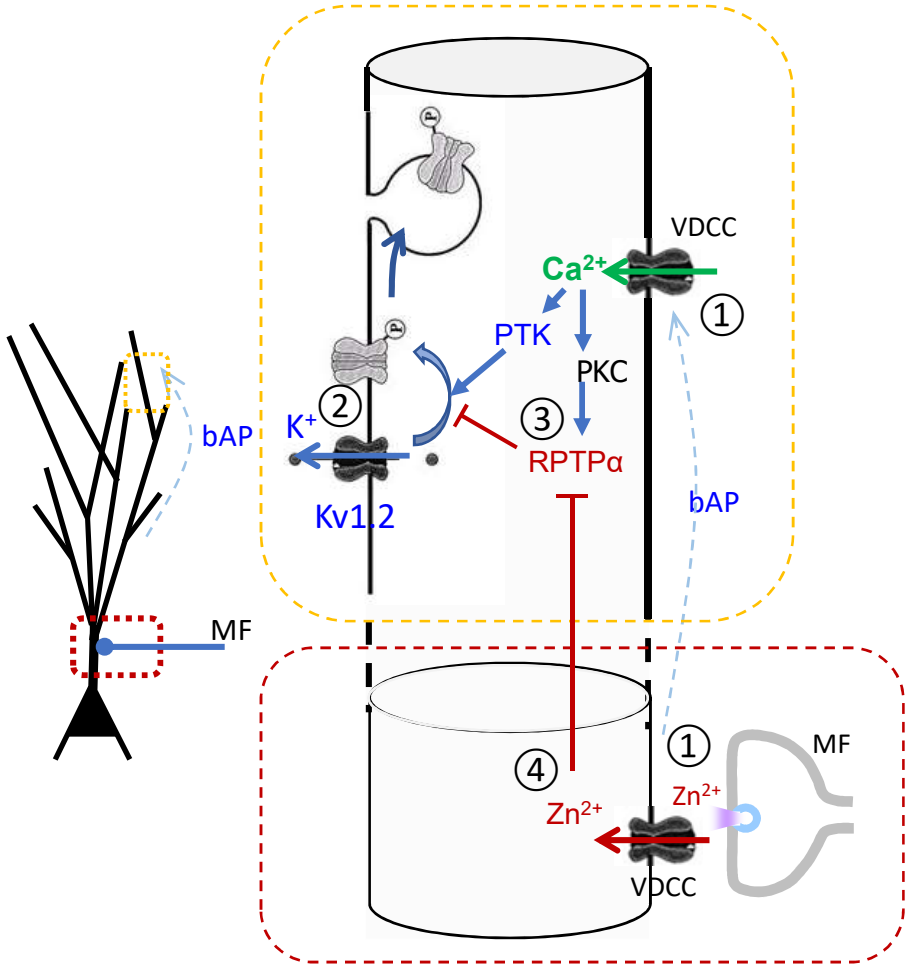

Fig. S2

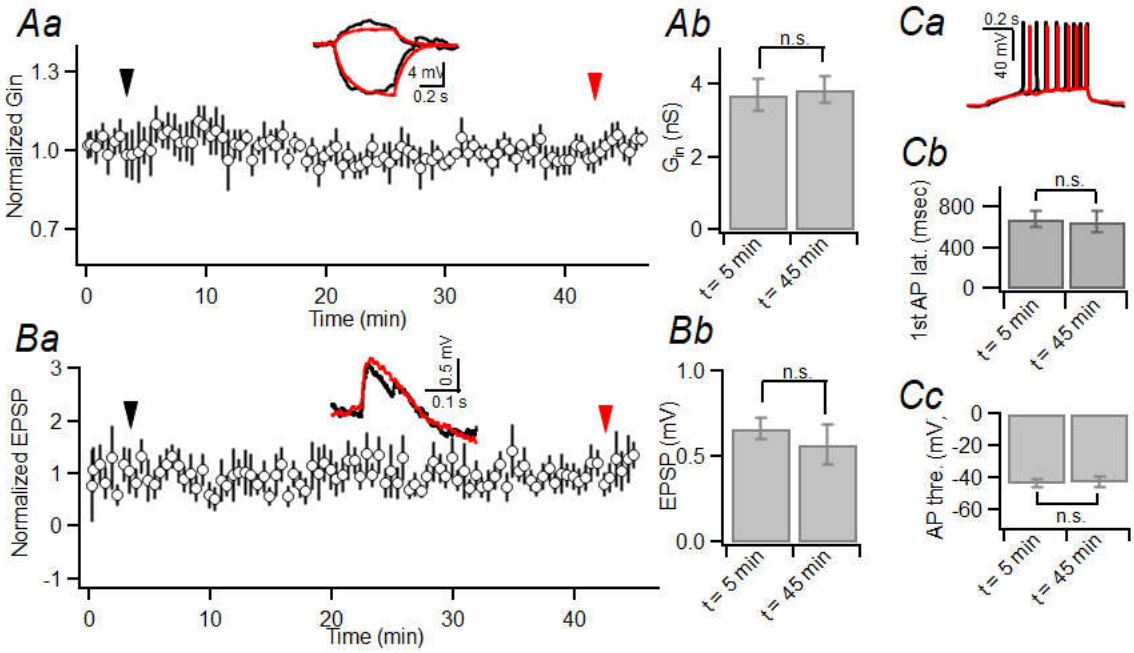
Aa
Normalized Gin
1.3
1.0
0.7
4 mV
0.2 s
0
10
20
30
40
Time (min)
Ab
n.s.
G_{in} (nS)
4
2
0
t= 5 min
t= 45 min
Ca
0.2 s
40 mV
Cb
n.s.
1st AP lat. (msec)
800
400
0
t= 5 min
t= 45 min
Ba
Normalized EPSP
3
2
1
0
-1
0.5 mV
0.1 s
0
10
20
30
40
Time (min)
Bb
n.s.
EPSP (mV)
1.0
0.5
0.0
t= 5 min
t= 45 min
Cc
AP thre. (mV)
0
-20
-40
-60
n.s.
t= 5 min
t= 45 min

Fig. S3

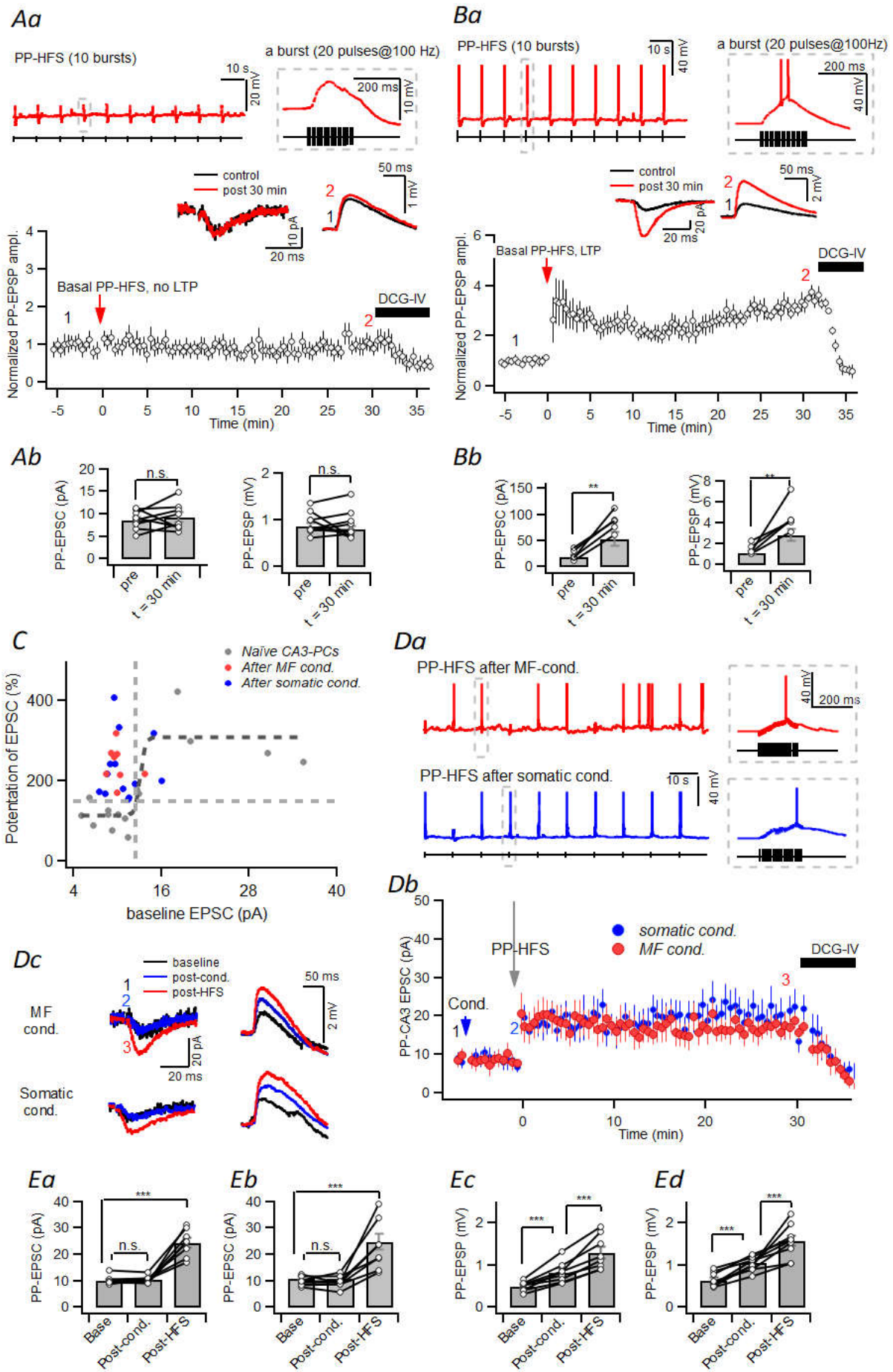
Aa
PP-HFS (10 bursts)
a burst (20 pulses@100 Hz)
control
post 30 min
Basal PP-HFS, no LTP
DCG-IV
Normalized PP-EPSP ampl.
Time (min)
Ba
PP-HFS (10 bursts)
a burst (20 pulses@100Hz)
Basal PP-HFS, LTP
Ab
PP-EPSC (pA)
PP-EPSP (mV)
n.s.
pre
t = 30 min
Bb
C
Naïve CA3-PCs
After MF cond.
After somatic cond.
Potentation of EPSC (%)
baseline EPSC (pA)
Da
PP-HFS after MF-cond.
PP-HFS after somatic cond.
Db
PP-HFS
Cond.
somatic cond.
MF cond.
PP-CA3 EPSC (pA)
Dc
baseline
post-cond.
post-HFS
MF cond.
Somatic cond.
Ea
Eb
Ec
Ed
Base
Post-cond.
Post-HFS

Fig. S4

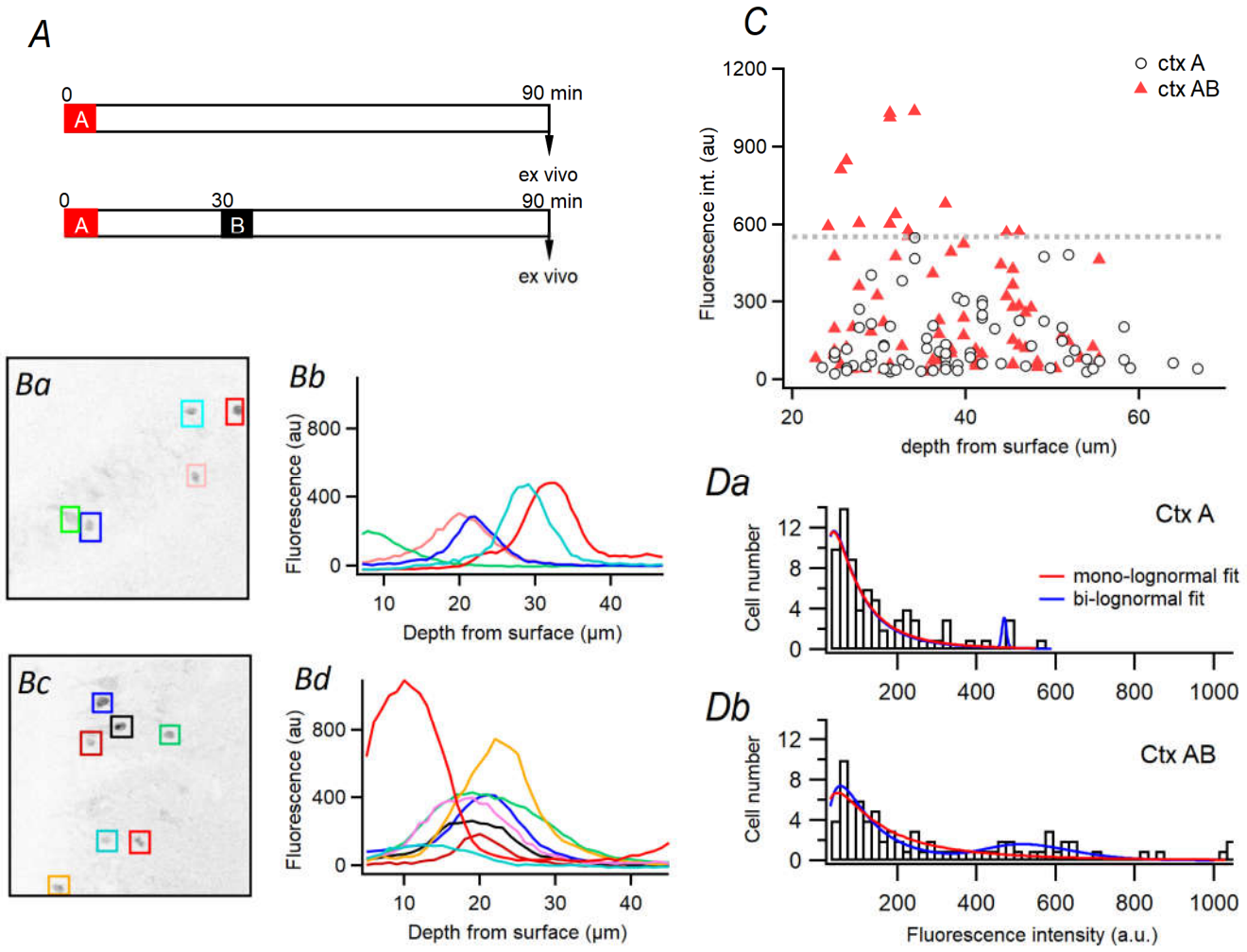
A
0
90 min
A
ex vivo
0
30
90 min
A
B
ex vivo
Ba
Bb
Fluorescence (au)
800
400
0
10
20
30
40
Depth from surface (µm)
Bc
Bd
Fluorescence (au)
800
400
0
10
20
30
40
Depth from surface (µm)
C
ctx A
ctx AB
Fluorescence int. (au)
1200
900
600
300
0
20
40
60
depth from surface (um)
Da
Ctx A
Cell number
12
8
4
0
mono-lognormal fit
bi-lognormal fit
200
400
600
800
1000
Db
Ctx AB
Cell number
12
8
4
0
200
400
600
800
1000
Fluorescence intensity (a.u.)

Fig. S5

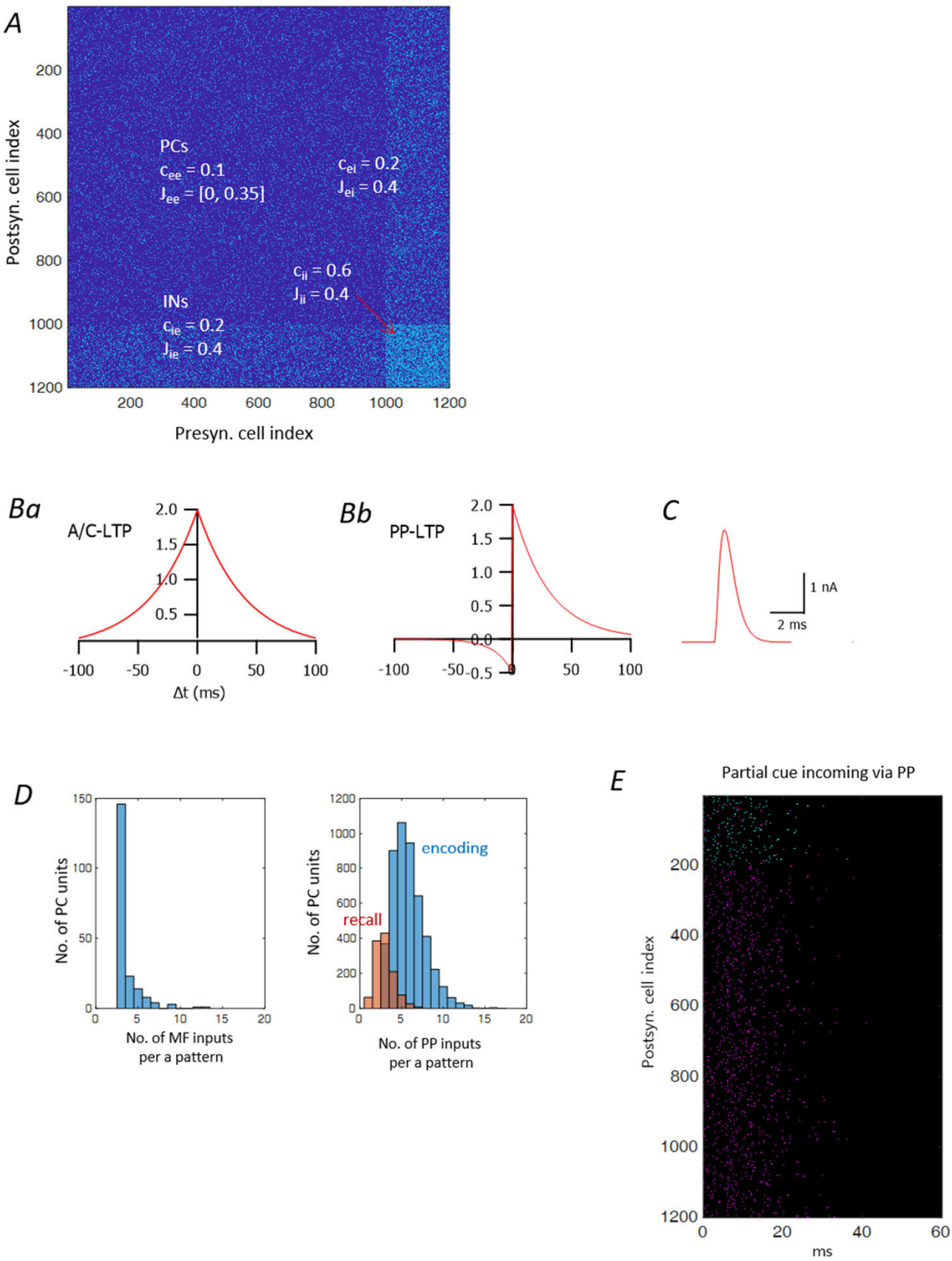
A
PCs
c_{ee} = 0.1
J_{ee} = [0, 0.35]
c_{ei} = 0.2
J_{ei} = 0.4
c_{ii} = 0.6
J_{ii} = 0.4
INs
c_{ie} = 0.2
J_{ie} = 0.4
Postsyn. cell index
Presyn. cell index
Ba
A/C-LTP
Δt (ms)
Bb
PP-LTP
C
1 nA
2 ms
D
No. of PC units
No. of MF inputs per a pattern
encoding
recall
No. of PP inputs per a pattern
E
Partial cue incoming via PP
Postsyn. cell index
ms